



The Type IIn Supernova SN 2010bt: The Explosion of a Star in Outburst

Nancy Elias-Rosa^{1,2}, Schuyler D. Van Dyk³, Stefano Benetti¹, Enrico Cappellaro¹, Nathan Smith⁴, Rubina Kotak⁵, Massimo Turatto¹, Alexei V. Filippenko^{6,7,16}, Giuliano Pignata^{8,9}, Ori D. Fox¹⁰, Lluís Galbany¹¹, Santiago González-Gaitán¹², Matteo Miluzio¹³, L. A. G. Monard¹⁴, and Mattias Ergon¹⁵

¹ INAF—Osservatorio Astronomico di Padova, vicolo dell’Osservatorio 5, Padova I-35122, Italy; eliasrosa.astro@gmail.com

² Institut de Ciències de l’Espai (CSIC-IEEC), Campus UAB, Camí de Can Magrans S/N, E-08193 Cerdanyola (Barcelona), Spain

³ Caltech/IPAC, Mailcode 100-22, Pasadena, CA 91125, USA

⁴ Steward Observatory, University of Arizona, Tucson, AZ 85720, USA

⁵ Astrophysics Research Centre, School of Mathematics and Physics, Queen’s University Belfast, Belfast BT7 1NN, UK

⁶ Department of Astronomy, University of California, Berkeley, CA 94720-3411, USA

⁷ Miller Institute for Basic Research in Science, University of California, Berkeley, CA 94720, USA

⁸ Departamento de Ciencias Físicas, Universidad Andres Bello, Avda. República 252, Santiago, 8320000, Chile

⁹ Millennium Institute of Astrophysics (MAS), Nuncio Monseñor Sótero Sanz 100, Providencia, Santiago, Chile

¹⁰ Space Telescope Science Institute, 3700 San Martin Drive, Baltimore, MD 21218, USA

¹¹ PITT PACC, Department of Physics and Astronomy, University of Pittsburgh, Pittsburgh, PA 15260, USA

¹² CENTRA, Departamento de Física, Instituto Superior Técnico, Universidade de Lisboa, Avenida Rovisco Pais 1, 1049 Lisboa, Portugal

¹³ European Space Astronomy Centre (ESAC), European Space Agency, Villanueva de la Cañada, Madrid, E-28692, Spain

¹⁴ Kleinkaroo Observatory, Center for Backyard Astronomy Kleinkaroo, Sint Helena 1B, PO Box 281, Calitzdorp 6660, South Africa

¹⁵ The Oskar Klein Centre, Department of Astronomy, AlbaNova, Stockholm University, SE-10691 Stockholm, Sweden

Received 2017 September 20; revised 2018 April 25; accepted 2018 May 3; published 2018 June 13

Abstract

It is well known that massive stars ($M > 8 M_{\odot}$) evolve up to the collapse of the stellar core, resulting in most cases in a supernova (SN) explosion. Their heterogeneity is related mainly to different configurations of the progenitor star at the moment of the explosion and to their immediate environments. We present photometry and spectroscopy of SN 2010bt, which was classified as a Type IIn SN from a spectrum obtained soon after discovery and was observed extensively for about 2 months. After the seasonal interruption owing to its proximity to the Sun, the SN was below the detection threshold, indicative of a rapid luminosity decline. We can identify the likely progenitor with a very luminous star ($\log L/L_{\odot} \approx 7$) through comparison of *Hubble Space Telescope* images of the host galaxy prior to explosion with those of the SN obtained after maximum light. Such a luminosity is not expected for a quiescent star, but rather for a massive star in an active phase. This progenitor candidate was later confirmed via images taken in 2015 (~ 5 yr post-discovery), in which no bright point source was detected at the SN position. Given these results and the SN behavior, we conclude that SN 2010bt was likely a Type IIn SN and that its progenitor was a massive star that experienced an outburst shortly before the final explosion, leading to a dense H-rich circumstellar environment around the SN progenitor.

Key words: galaxies: individual (NGC 7130) – stars: evolution – supernovae: general – supernovae: individual (SN 2010bt)

Supporting material: data behind figure, machine-readable table

1. Introduction

Type II “narrow” (IIn) supernovae (SNe) are a heterogeneous subset of core-collapse SNe (CC-SNe; Schlegel 1990). According to Li et al. (2011) and Smith et al. (2011a), they represent 9% of all CC-SNe and seem to preferentially occur in small and late-type spiral galaxies.

This subclass of objects can be distinguished from other types of CC-SNe by their spectral appearance. On the other hand, they can also be confused with nonterminal outbursts of very massive stars. The broad absorption lines typical of many SNe are weak or absent in SNe IIn throughout their evolution. Instead, they show strong, narrow Balmer emission components (with FWHM intensity ranging from a few tens to a few hundreds of km s^{-1}) atop broader emission (which can have intermediate-velocity components with FWHM $\approx 1000 \text{ km s}^{-1}$, as well as broad components with FWHM of a few thousands of km s^{-1} ; see, e.g., Filippenko 1997). The narrow lines are thought to arise from the surrounding circumstellar material (CSM) ionized by the shock-

interaction emission (e.g., Chugai & Danziger 1994). Their light curves, however, exhibit a wide range of properties (see, e.g., Smith 2017). This diversity is related to the mass-loss history during the evolution of massive stars.

It was suggested that the progenitors of a fraction of these interacting SNe are massive stars in a luminous blue variable (LBV) phase. These stars are among the most luminous ($M_{\text{bol}} < -9.6$ mag) and massive ($> 50 M_{\odot}$) stars in late-type galaxies (e.g., Humphreys & Davidson 1994). The evidence arises from the identification of the progenitor stars of a few SNe IIn, such as SN 2005gl (Gal-Yam et al. 2007; Gal-Yam & Leonard 2009), SN 2009ip (Smith et al. 2010, 2014; Foley et al. 2011), and SN 2015bh (Elias-Rosa et al. 2016; Thöne et al. 2017). A luminous, blue point-like source, originating from either a young cluster or a single star, was first proposed as the progenitor of SN 2010jl by Smith et al. (2011b). Subsequently, Fox et al. (2017) argued that this source was most likely a massive young cluster, although they did not rule out the possibility of a very luminous progenitor star obscured by dust (see also Dwek et al. 2017). However, the nature of these progenitors is not fully clear, and other precursor

¹⁶ Miller Senior Fellow.

channels have been proposed (see, e.g., Mauerhan & Smith (2012) in the case of the SN 1998S, or Smith (2014) for a larger review of this topic).

As mentioned above, the powerful nonterminal outbursts of very massive stars can mimic genuine SN explosions, in terms of energetics and spectral appearance (both show incipient narrow lines of hydrogen in emission); thus, they are usually referred to as ‘‘SN impostors’’ (e.g., SN 1997bs, Van Dyk et al. 2000; SN 2000ch, Pastorello et al. 2010; see also the general discussions in Smith et al. 2011c; Van Dyk & Matheson 2012). Discriminating between SN impostors and SNe IIn is challenging, and for several objects both possibilities remain viable (see, e.g., the case of SN 2007sv; Tartaglia et al. 2015).

SN 2010bt was discovered in NGC 7130 on 2010 April 17.11 (UT dates are used throughout this paper) at an unfiltered magnitude of 15.9 and confirmed on 2010 April 18.14 at a magnitude of 15.8 (Monard 2010; Figure 1). The presence of Balmer emission with multicomponent profiles in the spectrum from 2010 April 18.39 led to the classification of SN 2010bt as an SN IIn, a few days after discovery (Turatto et al. 2010).

NGC 7130 (or IC 5135; $z = 0.016^{17}$; morphological type Sa pec) was classified as a Seyfert 2 galaxy by Phillips et al. (1983)—i.e., an active galactic nucleus (AGN) with obscuring material that precludes a direct view of its nuclear region. Throughout the paper, we adopt a distance to NGC 7130 of 65.4 ± 4.6 Mpc ($\mu = 34.08 \pm 0.15$ mag), resulting from the recession velocity of the galaxy (de Vaucouleurs et al. 1976) corrected for Local Group infall into the Virgo Cluster (Mould et al. 2000), $v_{\text{vir}} = 4771 \pm 17$ km s $^{-1}$ ($z = 0.016$), assuming $H_0 = 73$ km s $^{-1}$ Mpc $^{-1}$ (values taken from NED).

This paper presents and discusses our photometric and spectroscopic observations of SN 2010bt in Section 2. In Section 3, we compare pixel by pixel four sets of *Hubble Space Telescope* (*HST*) data, and we discuss the nature of the progenitor star in Section 4. We conclude in Section 6.

2. The Nature of SN 2010bt

2.1. Photometry

Optical *BVRI* images of SN 2010bt were obtained with the 1.3 m Small and Moderate Aperture Research Telescope System (SMARTS)+ANDICAM at Cerro Tololo Inter-American Observatory (CTIO), the 6.5 m Magellan Clay Telescope +LDSS-3 at Las Campanas Observatory, and the 3.58 m New Technology Telescope (NTT)+EFOSC2 at the European Southern Observatory (ESO) of La Silla Observatory, all located in Chile. The data were obtained thanks to a collaboration between American and European researchers. We also include in our data set unfiltered data from the Bronberg Observatory (South Africa) and archival images from the 1.0 m Jacobus Kapteyn Telescope at Roque de Los Muchachos Observatory (Spain). More information about the telescopes and instruments used in this follow-up campaign can be found in Table 1.

The photometric observations were processed following the standard recipe in IRAF for CCD images (trimming, overscan, bias, and flat-field corrections). Due to the location of SN 2010bt in NGC 7130, contamination of the SN photometry by the host-galaxy light was a serious problem. We therefore

used the template-subtraction technique to remove this background and hence to measure more accurately the SN magnitudes. The template images of NGC 7130 were obtained with the 1.3 m SMARTS telescope+ANDICAM at CTIO on 2011 August 03. Each SN image was registered geometrically and photometrically with its corresponding template using a dedicated pipeline (SNOOPY). This consists of a collection of PYTHON scripts calling standard IRAF tasks (through PYRAF) and other specific analysis tools, in particular SEXTRACTOR, for source extraction and star/galaxy separation. The instrumental magnitudes of the SN and the reference stars in the SN field were measured in the subtracted images (produced with HOTPANTS) using the point-spread function (PSF) fitting technique with the DAOPHOT package. In order to calibrate the instrumental magnitudes to the standard photometric VEGAMAG system, we used the magnitudes and colors of 15 local sequence stars in the SN field (Figure 1 and Table 2). The unfiltered data were transformed to the Johnson–Cousins *R* band, for which the effective wavelength is similar to the natural instrumental band defined by the CCD quantum efficiency of the detector that was used.

Near-infrared (NIR) observations were also obtained with the 3.6 m NTT+SOFI at the ESO Observatory of La Silla. We include in this work the data obtained at the 8.2 m unit telescope UT4 of the Very Large Telescope+HAWK-I at the ESO Observatory of Cerro Paranal (PI: E. Cappellaro, 083.D-0259(A)), presented by Miluzio et al. (2013). The data were reduced using standard procedures for the VLT+HAWK-I data (see Miluzio et al. 2013, for details on the data reduction). For the NIR images we used two sets of images of the field as templates to subtract from the SN images, depending on the instrumentation, e.g., images from ESO NTT+SOFI taken on 2004 October 04 (PI: P. Lira, 074.B-0375(A)) and images from ESO VLT UT4+HAWK-I on 2011 April 24 (PI: E. Cappellaro, 083.D-0259(A)). The instrumental *JHK_s* photometry was calibrated using Two Micron All Sky Survey (2MASS¹⁸) stars in the field.

When the transient was not detected, upper limits were adopted corresponding to 2.5 times the standard deviation in the background. Uncertainty estimates were obtained through an artificial star experiment, combined (in quadrature) with the PSF fit error returned by DAOPHOT and the propagated uncertainties from the photometric calibration.

The final VEGAMAG calibrated magnitudes of SN 2010bt are listed in Tables 3 and 4. The single epoch with magnitudes in the Sloan system was transformed to the VEGAMAG system and included in Table 3 by employing the relations given by Blanton & Roweis (2007).

Space-based optical and ultraviolet (UV) data taken with the Ultraviolet/Optical Telescope (UVOT) on board *Swift* complement our ground-based photometry. The calibrated SN images in the UVOT-Vega system were obtained from SOUSA (*Swift*’s Optical/Ultraviolet Supernova Archive; Brown et al. 2014). Upper limits corresponding to three times the standard deviation in the background were estimated when the transient was not detected. The *Swift* photometry for SN 2010bt is reported in Table 5.

Finally, *HST* observed the SN 2010bt field at four epochs: 1994, 2003, 2010, and 2015 (see Sections 3 and 4 for more

¹⁷ NED, NASA/IPAC Extragalactic Database; <http://www.ipac.caltech.edu/>.

¹⁸ <http://www.ipac.caltech.edu/2mass/>

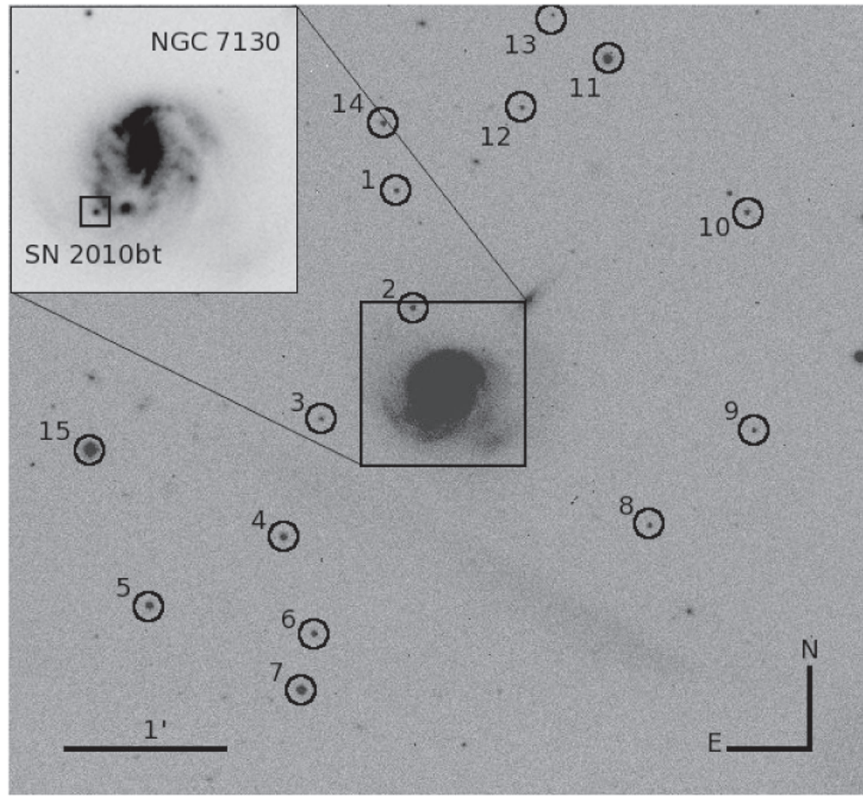


Figure 1. V-band image of SN 2010bt in NGC 7130 obtained with the 1.3 m SMARTS telescope+ANDICAM at CTIO on 2010 May 18 (field of view $\sim 6' \times 6'$). The SN and local photometric sequence stars are indicated.

Table 1
Basic Information about Telescopes and Instruments Used

Table Key ^a	Telescope	Instrument	Pixel Scale (arcsec pixel ⁻¹)	Location
ANDICAM	1.3 m SMARTS ^b	ANDICAM	0.37	CTIO, ^c Chile
BO	0.3 m Meade RCX400 <i>f</i> /8 telescope	SBIG ST8-XME CCD	1.37	Bronberg Observatory, South Africa
EFOSC2	3.6 m New Technology Telescope	EFOSC2	0.12	ESO, ^d La Silla Obs., Chile
HAWK-I	8.2 m Very Large Telescope UT4	HAWK-I	0.11	ESO, La Silla Obs., Chile
<i>HST</i> _WFPC2	2.4 m <i>HST</i>	WFPC2	0.05 ^e	...
<i>HST</i> _ACS/HRC	2.4 m <i>HST</i>	ACS/HRC	0.03	...
<i>HST</i> _ACS/WFC	2.4 m <i>HST</i>	ACS/WFC	0.05	...
<i>HST</i> _WFC3	2.4 m <i>HST</i>	WFC3/UVIS	0.04	...
JAG	1.0 m Jacobus Kapteyn Telescope	JAG ^f	0.33	ORM, ^g La Palma, Spain
LDSS-3	6.5 m Magellan Clay Telescope	LDSS-3	0.19	Las Campanas Obs., Chile
SOFI	3.6 m New Technology Telescope	SOFI	0.29	ESO, La Silla Obs., Chile
Spitzer	0.8 m <i>Spitzer Space Telescope</i>	IRAC	0.60	...
Swift	0.3 m Ritchey–Chrétien UV/optical Telesc.	<i>Swift</i>	0.50	...

Notes.

^a See Tables 3–5.

^b Small and Moderate Aperture Research Telescope System.

^c Cerro Tololo Inter-American Observatory.

^d European Southern Observatory.

^e WFPC2 contains four chips. The SN 2010bt field was observed with the Planetary Camera (0^{''}.05 pixel⁻¹).

^f JKT Acquisition and Guidance Unit.

^g Observatorio del Roque de los Muchachos.

details). The VEGAMAG magnitudes of the progenitor candidate and transient were obtained using Dolphot (see Table 10).

SN 2010bt was observed during the first ~ 50 (optical) to 80 (NIR) days after discovery. Subsequently, it came too close to

the Sun's direction and was lost. The telescopes could point to the field again around 2 months after the last observation in the NIR; however, at that time the SN was no longer visible (at least with ground-based telescopes). Instead, it was detected in

Table 2
Magnitudes of the Local Comparison Stars^a

Star	<i>B</i> (mag)	<i>V</i> (mag)	<i>R</i> (mag)	<i>I</i> (mag)	<i>J</i> (mag)	<i>H</i> (mag)	<i>K</i> (mag)
1	19.86 (0.07)	19.04 (0.05)	18.51 (0.03)	17.96 (0.04)
2	20.24 (0.07)	18.70 (0.05)	17.60 (0.07)	16.19 (0.04)	14.81 (0.03)	14.14 (0.02)	13.85 (0.04)
3	21.28 (0.07)	19.66 (0.04)	18.30 (0.04)	16.51 (0.05)	14.84 (0.03)	14.20 (0.04)	13.92 (0.05)
4	18.68 (0.04)	17.80 (0.04)	17.20 (0.03)	16.62 (0.03)	15.91 (0.07)	15.40 (0.09)	15.38 (0.13)
5	18.13 (0.04)	17.40 (0.03)	16.92 (0.02)	16.51 (0.03)	15.90 (0.07)	15.54 (0.08)	15.43 (0.14)
6	19.23 (0.04)	18.28 (0.04)	17.65 (0.04)	17.10 (0.03)	16.56 (0.11)	15.96 (0.11)	15.52 (0.17)
7	17.31 (0.03)	16.49 (0.03)	16.00 (0.03)	15.54 (0.03)	14.86 (0.03)	14.27 (0.04)	14.29 (0.05)
8	19.61 (0.05)	19.15 (0.06)	18.89 (0.04)	18.51 (0.04)
9	20.63 (0.04)	19.19 (0.04)	18.35 (0.04)	17.18 (0.04)	15.94 (0.06)	15.32 (0.07)	15.33 (0.13)
10	19.97 (0.06)	18.68 (0.03)	17.87 (0.03)	17.05 (0.02)	15.96 (0.08)	15.40 (0.07)	15.29 (0.13)
12	17.08 (0.03)	16.46 (0.02)	16.12 (0.04)	15.73 (0.02)	15.26 (0.04)	14.84 (0.05)	14.76 (0.09)
12	20.12 (0.04)	19.18 (0.05)	18.62 (0.05)	18.12 (0.07)
13	20.97 (0.03)	19.58 (0.01)	18.76 (0.02)	17.79 (0.04)	16.65 (0.11)	16.20 (0.15)	15.38 (0.15)
14	18.99 (0.04)	18.47 (0.04)	18.11 (0.04)	17.80 (0.03)
15	15.99 (0.04)	14.98 (0.03)	14.38 (0.06)	13.83 (0.05)	12.93 (0.03)	12.41 (0.02)	12.33 (0.03)

Note.

^a Quoted uncertainties are 1σ .

a F606W ($\sim V$ -) band *HST* exposure obtained ~ 175 days after discovery. The *UBVR_IJHK* light curves, including the *UBV*-*UVOT* data, are shown in Figure 2. In the figure, phase is relative to the discovery date on 2010 April 17.10, or MJD 55,303.1. However, in the following, and in order to better compare SN 2010bt with other SNe, we will refer to the *V* maximum computed as the discovery date minus 10 days (see Section 2.3 for more details).

As one can see in Figure 2, SN 2010bt was discovered after maximum light. The light curves show a decline similar to those of the rapidly declining SNe II studied by Anderson et al. (2014; with an average *V*-band light-curve decline > 1.3 mag in the first 50 days after peak). In fact, the *UBV* light curves of SN 2010bt show constant decline rates of 4.3, 4.0, and 3.3 mag/50 days,¹⁹ respectively, while the redder light curves (*R*) slightly flatten out in brightness around day 30 after SN discovery. The *K*-band light curve was also slowly declining (2.0 mag/50 days, considering the interval from ~ 38 to 80 days after the discovery date). SN 2010bt was only detected in two epochs in the *Swift* *UVW1* band, with a similar decline to that of the bluer light curves (~ 3.4 mag/50 days).

Figure 3 shows the evolution of the absolute *V* magnitude of SN 2010bt, compared with the SNe IIn SN 1996al (Benetti et al. 2016) and SN 1998S (Fassia et al. 2000; Liu et al. 2000; Pozzo et al. 2004) and the SN IIn/SN impostors SN 2009ip (Fraser et al. 2013; Mauerhan et al. 2013; Pastorello et al. 2013; Margutti et al. 2014) and SN 2015bh (Elias-Rosa et al. 2016). The comparison SNe have been corrected for extinction using published estimates and assuming the Cardelli et al. (1989) extinction law (see also Table 6). SN 2010bt exhibits a rapid decline at early times, similar to the decline from the “b” event of SN 2009ip and slightly faster than SN 1996al. This decline rate is also reminiscent of rapidly declining SNe II or even of SNe IIb (see, e.g., Li et al. 2011; Anderson et al. 2014). The absolute *V* magnitude at maximum of SN 2010bt was -19 mag or brighter, consistent with both the typical *V*-band peak magnitudes of

SNe IIn ($M_V = -18.4 \pm 1.0$ mag; Kiewe et al. 2012) and those of SNe II-P/L ($M_V = -16.89 \pm 0.98$ mag; Galbany et al. 2016).

The early-time $(B - V)_0$, $(V - R)_0$, and $(R - I)_0$ color curves of SN 2010bt (see Figure 4) exhibit rapid evolution from blue to red, similar to the color evolution of the other SNe IIn, yet different from SN 1996al.

We have computed the pseudobolometric light curve of SN 2010bt by integrating the flux at different wavelengths derived from the extinction-corrected optical apparent magnitudes over the sparse observations in the *UVW1* through *K* bands. Fluxes were measured considering only the epochs when *V*-band observations were available. When photometric measurements in one band at given epochs were not available, the flux was estimated by interpolating magnitudes from epochs close in time or, when necessary, by extrapolating the missing photometry assuming a constant color. We estimated the pseudobolometric flux at each epoch by integrating the spectral energy distribution (SED) using the trapezoidal rule and assuming zero flux outside the integration boundaries. Finally, the effective fluxes were converted to luminosities using the adopted distance to the SN (see Section 1). The errors in the bolometric luminosity include the uncertainties in the distance estimate, the extinction, and the apparent magnitudes. Note that the *UVW1* band provides about 13% of the luminosity.

In Figure 5 we present the pseudobolometric light curve of SN 2010bt, as well as those of SN 1996al, SN 1998S, SN 2009ip, and SN 2015bh computed with the same prescriptions (for SN 1996al and SN 1998S we have no observations in UV bands). As shown earlier, the luminosity decline of SN 2010bt is similar to that of SN 2009ip, while it was more luminous than all other SNe in the sample, with the possible exception of SN 1998S. Considering the first epoch in the *V* band for SN 2010bt, its peak may have reached a luminosity $> 1.3 \times 10^{43}$ erg s⁻¹ (SN 1998S had a luminosity at peak of 1.6×10^{43} erg s⁻¹).

Assuming that the tail of SN 2010bt followed the radioactive ⁵⁶Co decay with full trapping, and considering the explosion date to be between 15 and 50 days before the discovery date (see Section 2.3) and the *HST* detection in F606W ($\sim V$) at

¹⁹ Considering the interval from ~ 1 to 50 days after the discovery date.

Table 3
Optical Johnson–Cousins Photometry of SN 2010bt (VEGAMAG)^a

Date	MJD	Phase ^b (days)	<i>U</i> (mag)	<i>B</i> (mag)	<i>V</i> (mag)	<i>R</i> (mag)	<i>I</i> (mag)	Instrument Key
20010813	52,134.0	−3169.1	>18.0	...	JAG
20100417	55,303.1	0.0	16.00 (0.41)	...	BO
20100418	55,304.1	1.0	16.08 (0.18)	...	BO
20100418	55,304.4	1.3	...	17.00 (0.08)	16.33 (0.08)	16.05 (0.10)	15.79 (0.12)	EFOSC2
20100420	55,306.4	3.3	...	17.11 (0.03)	16.54 (0.03)	16.26 (0.04)	15.88 (0.04)	ANDICAM
20100420	55,306.9	3.8	16.88 (0.14)	17.33 (0.15)	16.58 (0.17)	<i>Swift</i>
20100422	55,308.1	5.0	17.09 (0.17)	17.35 (0.16)	16.42 (0.15)	<i>Swift</i>
20100423	55,309.4	6.2	...	17.42 (0.08)	16.81 (0.07)	16.50 (0.05)	16.17 (0.04)	ANDICAM
20100424	55,310.2	7.0	17.26 (0.19)	17.58 (0.18)	17.09 (0.24)	<i>Swift</i>
20100426	55,312.8	9.7	17.71 (0.26)	17.75 (0.22)	<i>Swift</i>
20100427	55,313.3	10.2	...	17.89 (0.18)	17.16 (0.16)	16.73 (0.09)	16.39 (0.14)	ANDICAM
20100428	55,314.7	11.6	17.71 (0.26)	17.77 (0.20)	17.25 (0.26)	<i>Swift</i>
20100430	55,316.0	12.9	>18.3	<i>Swift</i>
20100430	55,316.0	12.9	...	18.23 (0.28)	17.46 (0.30)	<i>Swift</i>
20100430	55,316.4	13.3	...	18.11 (0.15)	17.36 (0.13)	16.89 (0.10)	16.66 (0.09)	ANDICAM
20100501	55,317.9	14.7	>17.8	<i>Swift</i>
20100502	55,318.9	15.7	18.15 (0.35)	18.16 (0.27)	<i>Swift</i>
20100503	55,319.4	16.3	...	18.24 (0.14)	17.52 (0.12)	16.95 (0.09)	16.70 (0.10)	ANDICAM
20100504	55,320.9	17.8	18.27 (0.39)	18.46 (0.34)	17.69 (0.38)	<i>Swift</i>
20100506	55,322.1	19.0	17.18 (0.14)	...	BO
20100506	55,322.2	19.1	18.10 (0.35)	18.27 (0.30)	<i>Swift</i>
20100506	55,322.2	19.1	>17.7	<i>Swift</i>
20100507	55,323.4	20.2	...	18.56 (0.06)	17.79 (0.05)	17.30 (0.04)	16.96 (0.06)	ANDICAM
20100508	55,324.5	21.4	>18.3	>18.6	<i>Swift</i>
20100510	55,326.3	23.2	...	18.98 (0.13)	17.98 (0.11)	17.52 (0.06)	17.22 (0.06)	ANDICAM
20100511	55,327.1	24.0	>16.7	...	BO
20100518	55,334.4	31.3	...	19.58 (0.11)	18.59 (0.09)	17.98 (0.06)	17.69 (0.07)	ANDICAM
20100519	55,335.4	32.3	...	19.60 (0.08)	18.62 (0.07)	18.01 (0.06)	17.68 (0.06)	ANDICAM
20100523	55,339.3	36.2	...	19.84 (0.14)	18.84 (0.12)	18.19 (0.08)	17.91 (0.12)	ANDICAM
20100524	55,340.1	37.0	>16.5	...	BO
20100524	55,340.3	37.2	...	19.89 (0.14)	18.74 (0.12)	18.23 (0.11)	17.95 (0.12)	ANDICAM
20100526	55,342.3	39.2	...	20.10 (0.12)	19.04 (0.11)	18.34 (0.07)	18.03 (0.08)	ANDICAM
20100531	55,347.4	44.2	...	20.47 (0.13)	19.22 (0.12)	18.48 (0.07)	18.16 (0.09)	ANDICAM
20100604	55,351.3	48.2	...	20.79 (0.13)	19.48 (0.11)	18.63 (0.10)	18.24 (0.07)	ANDICAM
20100613	55,360.1	57.0	>16.6	...	BO
20100915	55,454.2	151.1	...	>19.8	>19.8	>18.9	>19.7	EFOSC2
20101004	55,473.1	170.0	...	>20.4	>20.0	>19.3	>18.7	EFOSC2
20101009	55,478.4	175.3	22.50 (0.05)	<i>HST_ACS/WFC</i>
20101028	55,497.2	194.1	...	>21.3	>21.0	>20.2	>19.7	EFOSC2
20150917	57,283.0	1979.9	...	>18.6	...	>18.5	...	LDSS-3
20151014	57,309.0	2005.9	>24.4	<i>HST_WFC3</i>

Notes.^a Quoted uncertainties are 1σ .^b Phases are relative to the discovery, MJD = 55,303.1.

(This table is available in its entirety in machine-readable form.)

Table 4
Near-infrared Photometry of SN 2010bt (VEGAMAG)^a

Date	MJD	Phase ^b (days)	<i>J</i> (mag)	<i>H</i> (mag)	<i>K</i> (mag)	Instrument Key
20100525	55,341.0	37.9	16.69 (0.23)	HAWK-I
20100606	55,353.0	49.9	17.51 (0.31)	HAWK-I
20100707	55,384.0	80.9	18.49 (0.22)	HAWK-I
20100917	55,456.1	153.0	>18.7	>17.4	>18.9	SOFI
20101029	55,498.1	195.0	>17.2	>15.4	...	SOFI

Notes.^a Quoted uncertainties are 1σ .^b Phases are relative to the discovery, MJD = 55,303.1.

Table 5
Swift UV Photometry of SN 2010bt (VEGAMAG)^a

Date	MJD	Phase ^b (days)	UVW1 (mag)	UVM2 (mag)	UVW2 (mag)
20100420	55,306.9	3.8	>18.5	>18.8	>18.9
20100422	55,308.1	5.0	18.20 (0.34)
20100422	55,308.2	5.0	...	>18.8	>18.9
20100424	55,310.2	7.0	18.48 (0.42)
20100424	55,310.2	7.0	...	>18.7	>18.9
20100426	55,312.8	9.7	>18.5	...	>18.4
20100428	55,314.7	11.6	>18.5	>18.3	>18.9
20100430	55,316.0	12.9	>18.6	>18.9	>19.0
20100502	55,318.9	15.7	>18.6	>18.9	>19.0
20100504	55,320.9	17.8	>18.5	>18.8	>18.9
20100506	55,322.2	19.1	>18.5	>18.9	>18.9
20100508	55,324.5	21.4	>18.5	>18.9	>18.9

Notes.

^a Quoted uncertainties are 1σ .

^b Phases are relative to the discovery, MJD = 55,303.1.

175.3 days (from discovery), we can roughly estimate $\leq 0.03 \pm 0.01 M_{\odot}$ for the ^{56}Ni mass, using the formula given by Hamuy (2003). This value is at the low end in comparison with typical values for CC-SNe, 0.001–0.3 M_{\odot} (Hamuy 2003). The ^{56}Ni mass of SN 2010bt is also in agreement with what was estimated for the interacting SN 1996al, SN 2009ip, and SN 2015bh ($M_{\text{Ni}} \leq 0.02$, ≤ 0.08 , and $\leq 0.04 M_{\odot}$, respectively; Fraser et al. 2013; Margutti et al. 2014; Smith et al. 2014; Benetti et al. 2016; Elias-Rosa et al. 2016).

2.2. Spectroscopy

Four low-resolution optical spectra of SN 2010bt were obtained on 2010 April 18 (classification spectrum), September 15 and 16, and October 28 with the 3.58 m NTT+EFOSC2 at ESO of La Silla (Chile). Only the first spectrum was taken with the slit along the parallactic angle to avoid differential flux losses (Filippenko 1982). For the other spectra it was necessary to point to a nearby bright star and then rotate the slit to position the SN 2010bt site inside the aperture. Basic information on our spectra is reported in Table 7.

All spectra were reduced following standard procedures with IRAF routines. The 2D spectroscopic frames were debiased and flat-fielded, before the optimized extraction (Horne 1986) of the 1D spectra. Wavelength calibration was accomplished with the help of arc-lamp exposures obtained the same night. Small adjustments estimated from night-sky lines in the object frames were applied. The spectra were flux-calibrated using the well-exposed continua of spectrophotometric standard stars (Oke 1990; Hamuy et al. 1992, 1994). An atmospheric extinction correction was applied using tabulated extinction coefficients for the ESO-La Silla Observatory. The strongest telluric absorption bands were removed using the standard-star spectra. Finally, the flux of each spectrum was cross-checked against the photometry.

Figure 6 shows the sequence of optical spectra of SN 2010bt,²⁰ and in Figures 7 and 8 we compare some of these spectra with those of SNe IIn SN 1996al (Benetti et al. 2016) and SN 1998S (Leonard et al. 2000) and the transients SN 2009ip (Fraser et al. 2013; Pastorello et al. 2013)

²⁰ Our spectra are available on WiseREP (Yaron & Gal-Yam 2012).

and SN 2015bh (Elias-Rosa et al. 2016) at similar epochs. All of the spectra have been corrected for extinction and deredshifted using values from the literature (see also Table 6).

The early-time spectrum (Figure 6, top panel) exhibits a blue continuum, with relatively weak spectral features, except for the strong Balmer emission lines with complex yet relatively narrow profiles. SN 2010bt does not show signs of the blue pseudocontinuum that characterizes some of the most energetic SNe IIn such as SN 1988Z (Turatto et al. 1993; Kiewe et al. 2012). The pseudocontinuum is a “blue excess” arising from the overlap of emission lines when the expanding ejecta of the SN interact with the surrounding CSM. The lack of a pseudocontinuum indicates that for SN 2010bt the continuum is thermal with a blackbody-like behavior.

Balmer emission lines show P Cygni absorption components with expansion velocities of 4000–3500 km s^{-1} , estimated from their absorption minima. A blend of He I $\lambda 5876$ and Na I D is also visible in the spectrum, with the broad emission centered at $\sim 5950 \text{ \AA}$ and with a very broad FWHM $\approx 290 \text{ \AA}$. The photospheric temperature at this epoch, estimated by fitting the SED of SN 2010bt with a blackbody function, is around 12,900 K (see also Table 8). Given this temperature and the pseudobolometric luminosity of SN 2010bt at that epoch, a radius of the photosphere of $\sim 8 \times 10^{14} \text{ cm}$ is inferred.

Consistent with the photometry, the $\text{H}\alpha$ profile of SN 2010bt resembles those of the interacting transients SN 2009ip and SN 2015bh and shows differences with SN 1996al and SN 1998S (see the close-up view of the $\text{H}\alpha$ profiles in Figures 7 and 8). The blackbody temperature shaping the continuum, though, is similar to that of SN 1998S, as are the strengths of the He I lines.

The extractions of the late-time spectra (>150 days) were arduous, given their low signal-to-noise ratio (S/N). Note that these spectra are contemporaneous with the upper photometric limits measured for SN 2010bt. The only distinct features are those of $\text{H}\beta$ and $\text{H}\alpha$, together with typical residual emission lines, such as [N II] $\lambda\lambda 6548, 6584$ and [S II] $\lambda\lambda 6717, 6731$, from neighboring H II regions. Despite the low S/N of the late-time SN 2010bt spectra, we notice some differences comparing its $\text{H}\alpha$ profile with that of the other SNe. None of the transients share the same profile shape, with that of SN 2010bt being double peaked yet narrower than that of the other objects (see the $\text{H}\alpha$ profiles magnified in Figure 8).

2.2.1. Hydrogen Feature Decomposition

The $\text{H}\alpha$ line profile of SN 2010bt appears to consist of multiple components with evident changes in morphology between early and late phases. We have decomposed the line into a Lorentzian profile for the narrow component and two Gaussian functions for the emission and absorption components of the broader P Cygni profile at the early epochs, and into two Lorentzian profiles for the oldest phases. To do this, we have used a Python script for least-squares minimization.

Figure 9 presents the $\text{H}\alpha$ emission line decomposition for three of our four epochs. The procedure independently fits the parameters, while the uncertainties were estimated using a bootstrap resampling technique, varying randomly the flux of each pixel according to a normal distribution having variance equal to the noise of the continuum. The velocities of the different gas components are listed in Table 8.

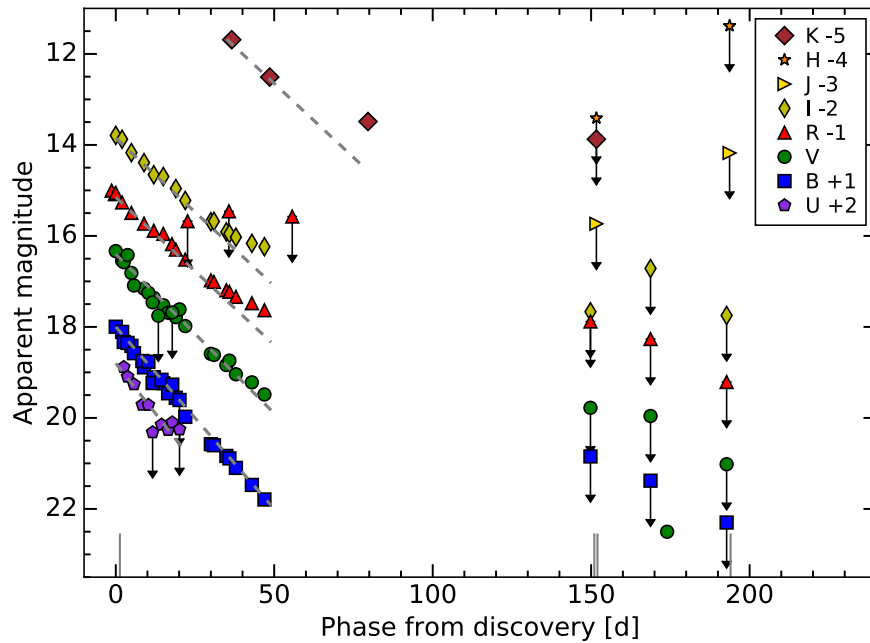


Figure 2. Optical and NIR light curves of SN 2010bt. Upper limits are indicated by symbols with arrows. The solid marks on the abscissa indicate the phases at which spectra were obtained. The dashed lines show the slopes of the light curves during the first 20 days from discovery. The light curves have been shifted for clarity by the amounts indicated in the legend. The uncertainties for most of the data points are smaller than the plotted symbols.

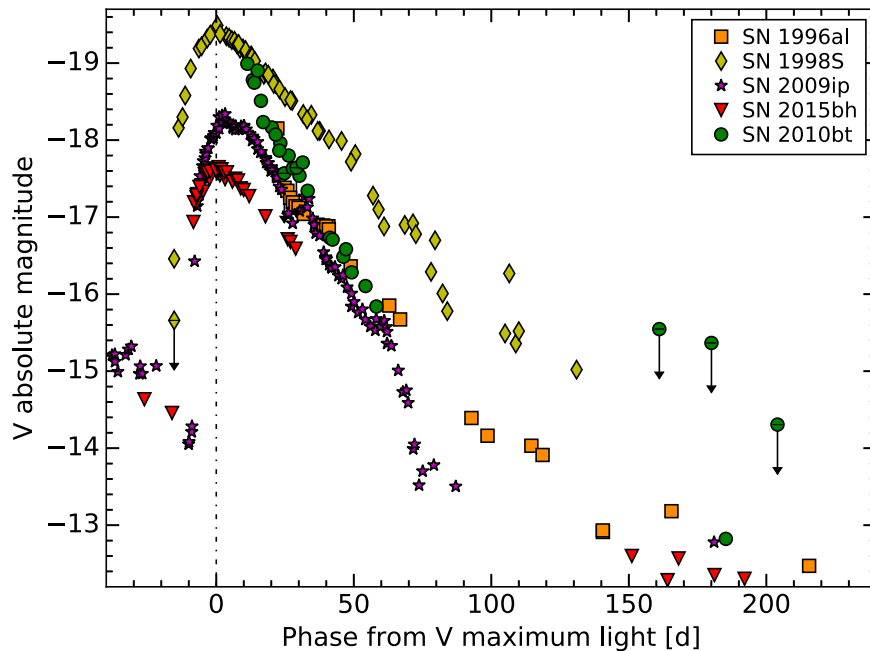


Figure 3. Absolute V light curve of SN 2010bt (circles), along with those of the SNe II in SN 1996al (squares) and SN 1998S (diamonds) and the controversial transients SN 2009ip (stars) and SN 2015bh (inverted triangles). Upper limits are indicated by symbols with arrows. The dot-dashed vertical line indicates the V -band maximum light of SN 2010bt. Ages are relative to V maximum light (we have assumed V maximum date = discovery date - 10 days, for SN 2010bt).

The relatively narrow $H\alpha$ emission at the first epoch (phase ~ 11.3 days) is resolved with an FWHM of $\sim 750 \text{ km s}^{-1}$ (after correction for instrumental resolution), while the broader component has $\text{FWHM} \approx 12,800 \text{ km s}^{-1}$. In addition, the blue side of the $H\alpha$ profile is “absorbed” by a P Cygni component with minimum at $\sim 3000 \text{ km s}^{-1}$. The broader component is redshifted, probably caused by electron scattering as the $H\alpha$ line photons diffuse through dense CSM ahead of the shock. The observed luminosity of $H\alpha$ was estimated from the integrated flux of the entire line to be $5 \times 10^{40} \text{ erg s}^{-1}$.

At later phases (>150 days), the $H\alpha$ profile is well reproduced with two Lorentzian components called “Blue” and “Rest,” given that they are centered at wavelengths of ~ 6542 and $\sim 6565 \text{ \AA}$, respectively. Clearly visible is a broad feature of $H\alpha$ in the 2D images of the late-time SN 2010bt spectra (see Figure 10). It is also evident that these spectra are likely contaminated by neighboring H II regions. In fact, a residual emission line centered at $\sim 6588 \text{ \AA}$, most likely corresponding to $[\text{N II}] \lambda 6584$, is present. Consequently, we have considered this line in the decomposition of $H\alpha$ by adding

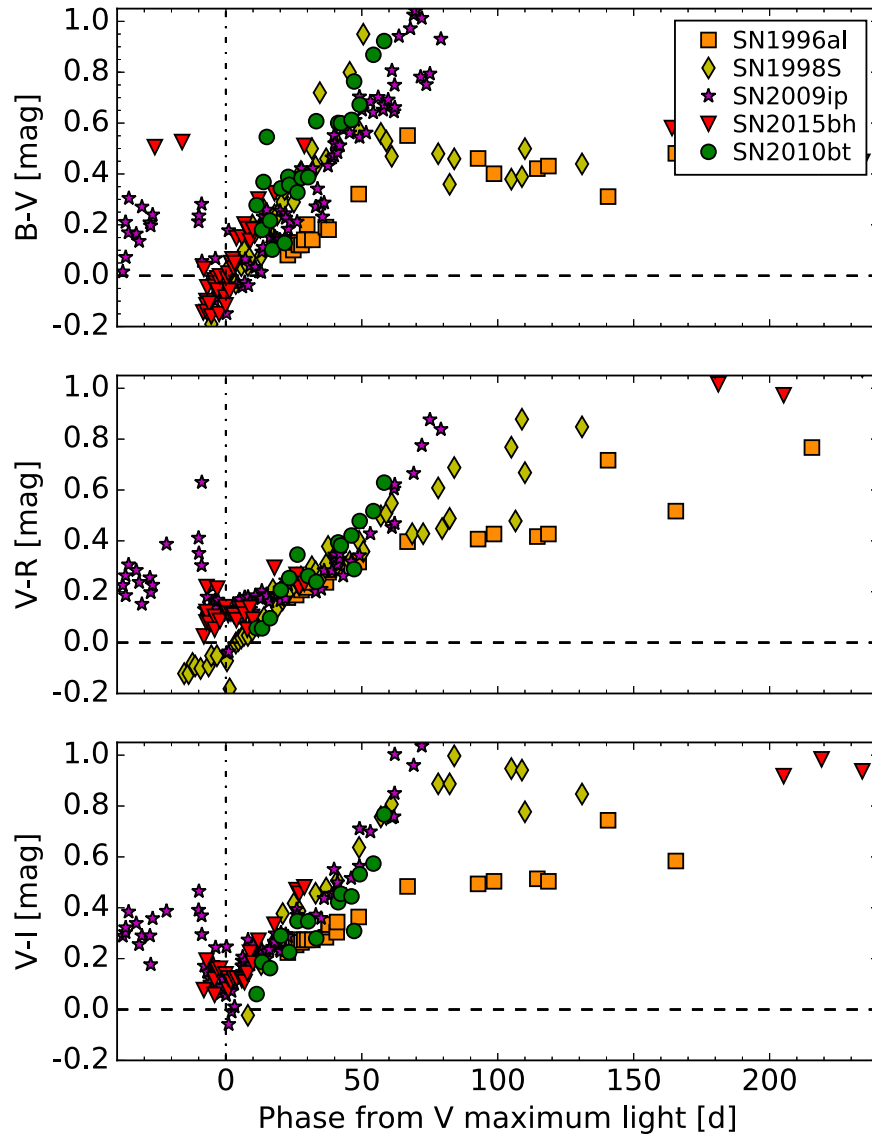


Figure 4. Intrinsic color curves of SN 2010bt (circles), compared with those of SN 1996al (squares), SN 1998S (diamonds), SN 2009ip (stars), and SN 2015bh (inverted triangles). The dot-dashed vertical line indicates the V -band maximum light of SN 2010bt. Ages are relative to V maximum light (we have assumed V maximum date = discovery date – 10 days, for SN 2010bt).

Table 6
Properties of the Comparison Supernovae

SN	Host Galaxy	Redshift	Distance ^a (Mpc)	$E(B - V)_{\text{tot}}$ (mag)	V_{max} Date (MJD)	Source
1996al	NGC 7689	0.007	22.9	0.110	50,265.0	a
1998S	NGC 3877	0.002	15.7	0.219	50,890.5	b
2009ip	NGC 7259	0.006	25.0	0.019	56,203.5	c
2015bh	NGC 2770	0.007	29.3	0.208	57,167.0	d
2010bt	NGC 7130	0.016	65.4 (4.6)	0.40 (0.14)	55,293.1 ^b	This work

Notes.

^a Distances have been scaled to $H_0 = 73 \text{ km s}^{-1} \text{ Mpc}^{-1}$.

^b We have assumed V maximum date = discovery date (MJD 55,303.1) – 10 days. Sources: (a) Benetti et al. (2016); (b) Fassia et al. (2000), Leonard et al. (2000), Pozzo et al. (2004), NED; (c) Pastorello et al. (2013), Fraser et al. (2013), Mauerhan et al. (2013), Margutti et al. (2014); (d) Elias-Rosa et al. (2016).

a third Lorentzian component. The FWHMs of the Blue and Rest components at all late epochs are relatively constant, at ~ 1500 and $\sim 1000 \text{ km s}^{-1}$, respectively. The total luminosity of the $H\alpha$ line at these phases decreases to $3 \times 10^{39} \text{ erg s}^{-1}$.

2.3. Explosion Date of SN 2010bt

Monard (2010) reported that no sources were visible at the SN position in images taken on 2009 December 22.80 (limit $> 17.8 \text{ mag}$, or $M_R \gtrsim -17.3 \text{ mag}$, for this particular case).

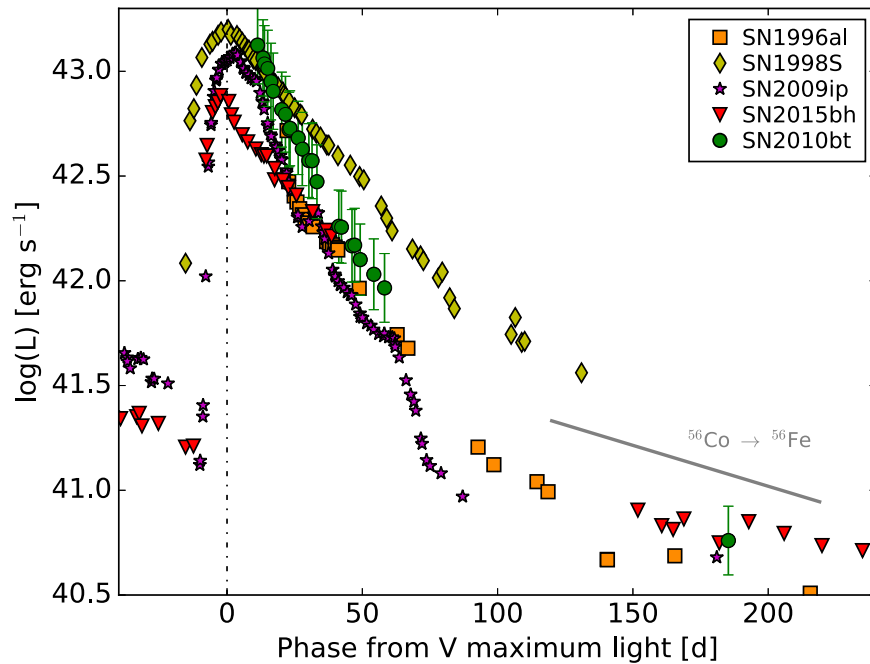


Figure 5. Pseudobolometric light curves of SN 2010bt (circles), compared with those of SN 1996al (squares), SN 1998S (diamonds), SN 2009ip (stars), and SN 2015bh (inverted triangles). The dot-dashed vertical line indicates the V -band maximum light of SN 2010bt. Ages are relative to V maximum light (we have assumed V maximum date = discovery date – 10 days, for SN 2010bt).

Table 7
Log of Spectroscopic Observations of SN 2010bt

UT Date	MJD	Phase ^a (days)	Instrument Key	Grism/Grating + slit	Spectral Range (Å)	Resolution (Å)
20100418	55304.4	1.3	EFOSC2	gm11+gm16+1''5	3400–10,300	14
20100915	55454.1	151.0	EFOSC2	gm11+gm16+1''0	3400–10,300	14
20100916	55455.1	152.0	EFOSC2	gm11+1''0	3400–7500	14
20101028	55497.1	194.0	EFOSC2	gm11+1''0	3400–7500	14

Note.

^a Phases are relative to the date of discovery, MJD = 55,303.1.

Nothing was also visible in a HAWK-I image taken on 2009 July 26.60 (limit $K > 19.0$ mag; in this case $M_K \gtrsim -15.2$ mag; Miluzio et al. 2013). Therefore, the SN explosion occurred less than 115 days before discovery.

A more accurate date of the explosion is difficult to estimate in the case of SN 2010bt. The main complications are the peculiar behaviors of both its photometric and spectroscopic evolution.

The light curves (see Section 2.1) show that the SN was discovered after maximum light. Assuming that the V -band light curve of SN 2010bt has a similar decay slope to that of SN 2009ip (see Section 2.1 and Figure 3), the former would have been discovered no more than 10 days after maximum light. This estimate is also confirmed by the behavior of the color curves. Considering that SNe II_n generally have a rise time of >5 days (Ofek et al. 2014), SN 2010bt would have exploded at least 15 days before the discovery. On the other hand, and according to the template-fitting code GELATO, acceptable matches with SNe II_n at phases between 10 and 50 days after explosion are found for the early-time SN 2010bt spectrum (although the best fit is at 10 days).

Thus, in view of all these uncertainties, we are able to determine only that the explosion occurred 15–50 days before discovery.

3. Identification of the Progenitor Candidate

In order to search for a possible SN progenitor, we isolated archival²¹ HST images of NGC 7130 taken with the Wide Field and Planetary Camera 2 (WFPC2) in $F606W$ ($\sim V$; 500 s exposure) on 1994 August 23 by program GO-5479 (PI: M. Malkan) and with the High Resolution Channel (HRC) of the Advanced Camera for Surveys (ACS) in $F330W$ ($\sim u$; 1200 s exposure) on 2003 May 08 by program GO-9379 (PI: H. Schmitt). We worked with drizzled images downloaded from the Hubble Legacy Archive.²² These images have been resampled to a uniform grid to correct for geometric distortions.

We performed relative astrometry by geometrically transforming the pre-explosion images to match those taken after the explosion. We first used the ground-based, post-explosion CTIO/SMARTS image taken on 2010 April 23 (with seeing $1''.5$) to approximately locate the position of the SN in the WFPC2 images. Then, we confirmed the identification of this candidate through high-resolution HST ACS images using the Wide Field Channel (WFC, $\sim 0''.05$ pixel⁻¹; a pair of observations of 40 and 80 s exposures), obtained through the $F606W$

²¹ <http://archive.stsci.edu/hst/>

²² <http://hla.stsci.edu/hlaview.html>

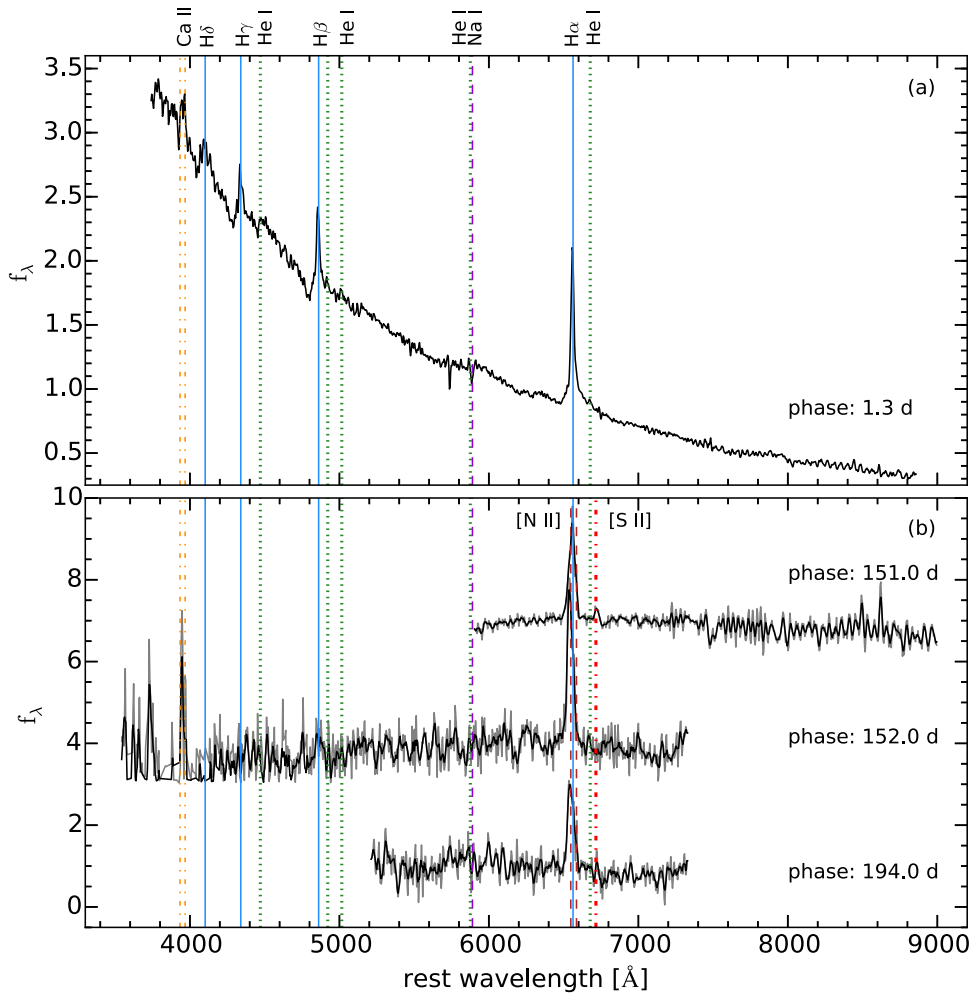


Figure 6. (a) Early-time and (b) late-time optical spectra of SN 2010bt. The late spectra are shown in gray, with a boxcar-smoothed (using a 5 pixel window) version of the spectra overlotted in black. The locations of the most prominent spectral features are indicated by vertical lines. The data used to create this figure are available.

filter on 2010 October 09, as part of our Target-of-Opportunity program GO-11575 (PI: S. Van Dyk). The individual exposures of this trigger were drizzled to produce a final mosaic. However, as we showed in Section 2.1, the SN was already quite faint at the time of these observations ($F606W(\sim V) = 22.5$ mag; see Table 3), leaving some ambiguity in its identification. Therefore, we used the *HST* post-explosion image to identify the progenitor in the pre-SN WFPC2 and ACS/HRC images, as follows.

(i) Initially, we obtained a precise SN position, at $\alpha = 21^{\text{h}}48^{\text{m}}20^{\text{s}}.28$, $\delta = -34^{\circ}57'17''.7$ (J2000.0), with rms uncertainties of $\sim 0''.1$, based on nine point-like sources as fiducials in the *V*-band NTT+EFOSC2 image taken on 2010 April 18. We measured the centroids of the fiducial sources with the IRAF tasks IMEXAMINE. We adopted the 2MASS Point Source Catalog as the astrometric grid and used the IRAF task CCMAP to obtain the solution. At that point, we were able to confirm the SN position in the *HST* post-explosion mosaic, with rms uncertainty $< 0''.06$, and located the faint SN.

(ii) Then, we achieved high-precision relative astrometry between the pre-explosion WFPC2 F606W (we worked only with the drizzled PC image, since the SN site is located on this chip, with $0''.045 \text{ pixel}^{-1}$) and ACS/HRC F330W images (with $\sim 0''.025 \text{ pixel}^{-1}$) and the post-explosion ACS/WFC image, by

geometrically transforming the former pair to match the latter. We used 17 point-like sources in common between the three sets of images and the IRAF task GEOMAP for the transformation.

The positions (and their uncertainties) for the SN and the progenitor candidate are obtained by averaging the measurements from two centroiding methods, the task DAOFIND within IRAF/DAOPHOT and IMEXAMINE within IRAF. As a result, in the pre-SN F606W image we identify an object very close to the SN position, which we consider to be the progenitor candidate. This same object is faintly detected at this position in the F303W image; see Figures 11(a) and (b). The pixel position for the SN transformed into the pre-SN F606W image is $[242.83, 363.79]$, while the candidate position is $[243.08, 363.96]$; for the pre-SN F330W image, these are $[348.36, 317.88]$ and $[348.92, 318.02]$, respectively. The differences between the SN and the progenitor candidate positions, compared with the total estimated astrometric uncertainty, are given in Table 9. The latter uncertainty was calculated as a quadrature sum of the uncertainties in the SN and progenitor candidate positions and the rms uncertainty in the geometric transformation.

From the results in Table 9, it can be seen that the difference between the SN position and the position of the progenitor

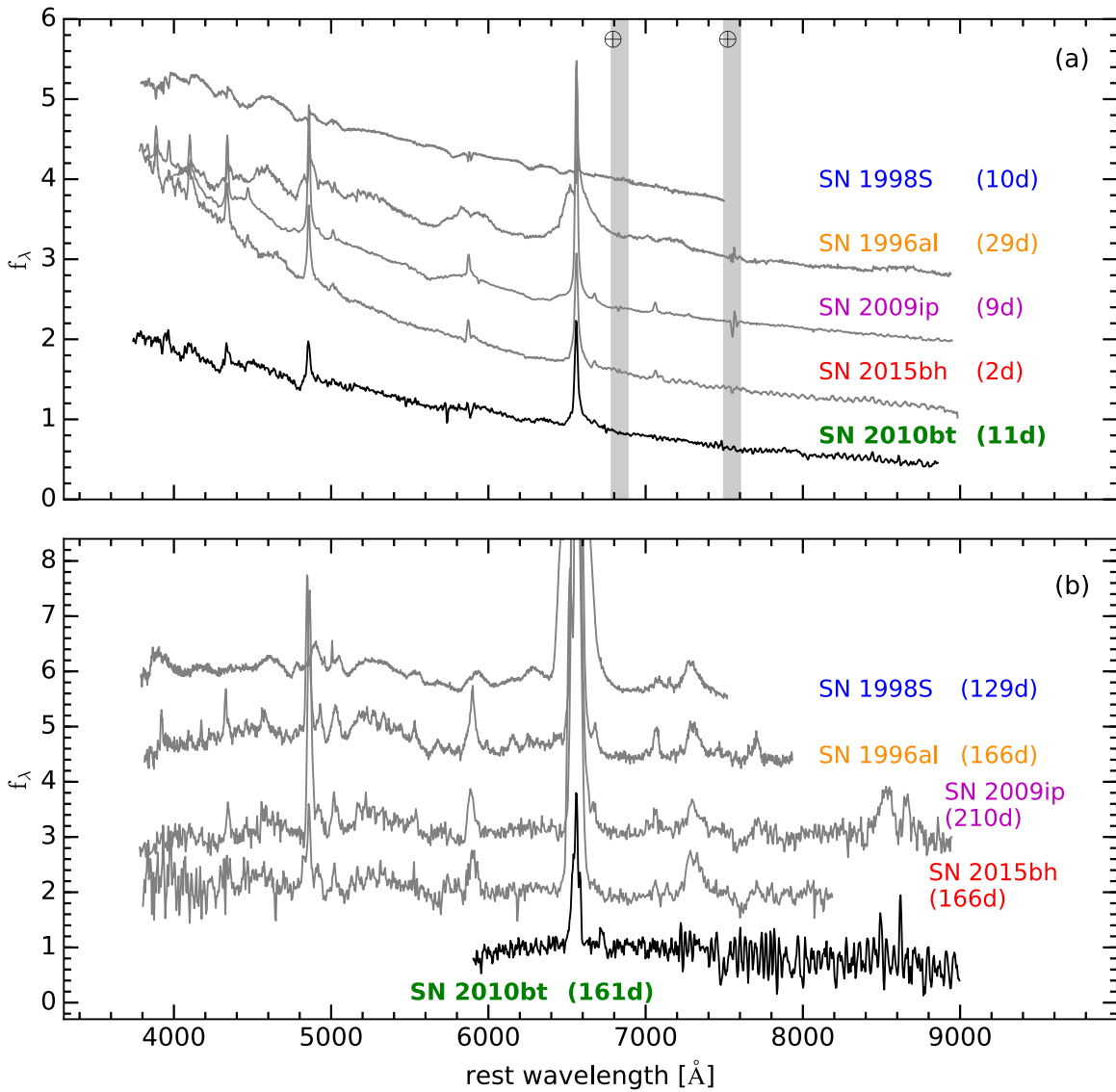


Figure 7. Comparison of SN 2010bt (a) early-time and (b) late-time optical spectra, along with those of the interacting SN 1996al, SN 1998S, SN 2009ip, and SN 2015bh at similar epochs. All spectra have been corrected for their host-galaxy recession velocities and for extinction (values adopted from the literature; see also Table 6). Ages are relative to V maximum light.

candidate is slightly larger in right ascension for both bands than the measurement uncertainties; the agreement is much better in declination. However, the differences in position are within 3σ of the total uncertainties. We therefore consider the candidate as the SN progenitor star and attribute the larger offset in right ascension (about 28 and 13 mas in F330W and F606W, respectively) to the complex background in the bright spiral arm of the host galaxy on which the progenitor candidate is located. We emphasize that no other point-like source exists within this 3σ radius from the progenitor candidate position (see Figure 11(c)).

The field was observed again on 2015 October 14 as part of our Target-of-Opportunity program GO-13683 (PI: S. Van Dyk). On this occasion we obtained six dithered images of 100 s exposure with the *HST* Wide Field Camera 3 (WFC3) UVIS channel ($\sim 0''.04 \text{ pixel}^{-1}$) in F555W band (hereafter labeled as “late-time *HST* images”). Using relative astrometry, we matched the observations of SN 2010bt before and after the explosion with this late-time drizzled *HST* image. We did not detect any luminous point source at the SN position in the

F555W image (Figure 11(d)), confirming the identification of the progenitor (see next section for further details).

4. The Nature of the Progenitor Candidate

As discussed in Section 2.2, the early-time spectrum of SN 2010bt has a rather blue continuum, yet it also exhibits relatively strong, narrow Na I D absorption, suggesting the simultaneous presence of dust and extinction suffered by the SN. Measuring the equivalent width (EW) of the blended Na I D line at the host-galaxy redshift ($z_0 = 0.016$) from the early-time optical spectrum of SN 2010bt ($\sim 1.8 \text{ \AA}$), we can attempt to estimate $E(B - V)_{\text{tot}}$. Any relationship between EW and $E(B - V)$ tends to break down for SNe with moderate to high reddening. We obtain a large dispersion in the results following the relations of different authors. Specifically, we estimate $E(B - V)_{\text{tot}} \approx 0.3$ and 0.9 mag (i.e., $A_V \approx 0.8$ and 2.7 mag, respectively—assuming the Cardelli et al. [1989] reddening law with updated wavelengths and $R_V = 3.1$) following Turatto et al. (2003) and $E(B - V)_{\text{tot}} \approx 1.6$ mag

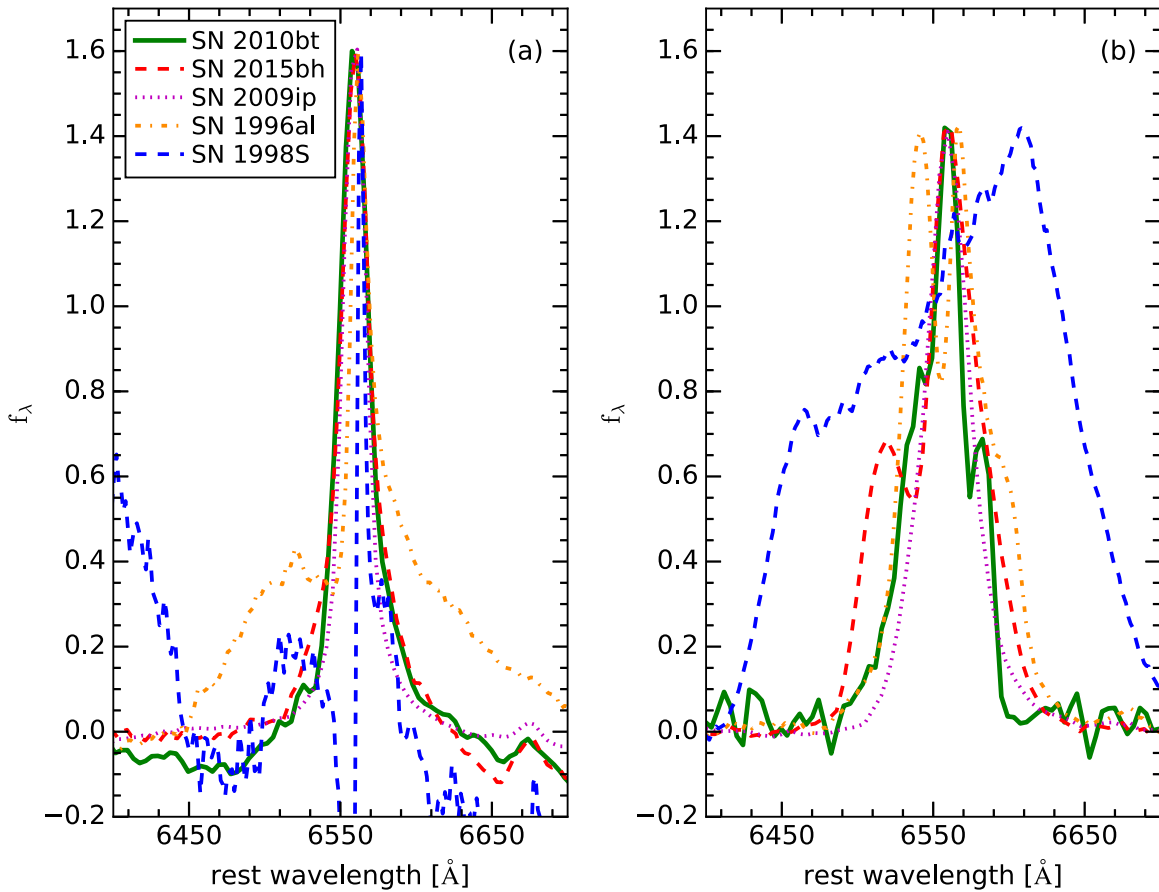


Figure 8. Close-up view of the H α profiles of the spectra in Figure 7. Panel (a) shows the early-time optical spectra, and panel (b) those taken at late times. The profiles are normalized to the same peak flux.

Table 8
Main Parameters Inferred from Spectra of SN 2010bt

UT Date	MJD	Phase ^a (days)	Temp. ^b (K)	Radius ^c (10^{14} cm)	FWHM _{Hα,nar} ^d (km s ⁻¹)	FWHM _{Hα,br} (km s ⁻¹)	v_{P-Cyg} (km s ⁻¹)	$L(H\alpha)$ (10^{30} erg s ⁻¹)
20100418	55,304.4	11.3	12900	8 (2)	750 (100)	12,800 (1600)	3000 (800)	50 (7)
					FWHM _{Blue} (km s ⁻¹)	FWHM _{Rest} (km s ⁻¹)		
20100915	55,454.1	161.0	1500 (400)	1050 (300)	...	3 (1)
20100916	55,455.1	162.0	1550 (400)	750 (500)	...	2 (1)
20101028	55,497.1	204.0	1450 (400)	1100 (350)	...	1 (0.4)

Notes.

^a Phases are relative to the assumed V maximum date = discovery date (MJD 55,303.1) – 10 days.

^b We consider a conservative uncertainty in the temperature of about ± 500 K.

^c We have propagated the uncertainties from the Stefan–Boltzmann equation.

^d The velocities are computed from the decomposition of the H α profile.

(i.e., $A_V \approx 5.0$ mag) using Poznanski et al. (2012). Because of the large differences obtained with the EW(NaID) versus $E(B - V)$ relations, we decided not to use this method to estimate the extinction toward SN 2010bt. Phillips et al. (2013) have also cautioned that the EW(NaID) versus $E(B - V)$ relationship is associated with large scatter.

Thus, in order to estimate a consistent value for the extinction (A_V) toward SN 2010bt, we considered different methods based on comparisons of the object’s SED and luminosity with those of other “standard” SNe II. It should be noted that in fact SNe II exhibit a wide diversity in both photometry and spectra (see, e.g.,

Kiewe et al. 2012; Taddia et al. 2013). We first matched simultaneously the intrinsic $(B - V)_0$, $(V - R)_0$, and $(R - I)_0$ color curves of SN 2010bt with those of other SNe II (see Figure 4), finding an extinction $A_V = 1.47 \pm 0.31$ mag. We also compared the early-time optical SED of SN 2010bt (we did not use the late-time spectra, given their comparatively poor S/N) with those of the interacting SN 1998S, SN 2009ip, and SN 2015bh at similar epochs. Spectra of the comparison SNe were first corrected for redshift and extinction and then scaled to the distance of SN 2010bt. The average of the good matches in all cases is $A_V = 0.98 \pm 0.33$ mag. We adopt the uncertainty-weighted

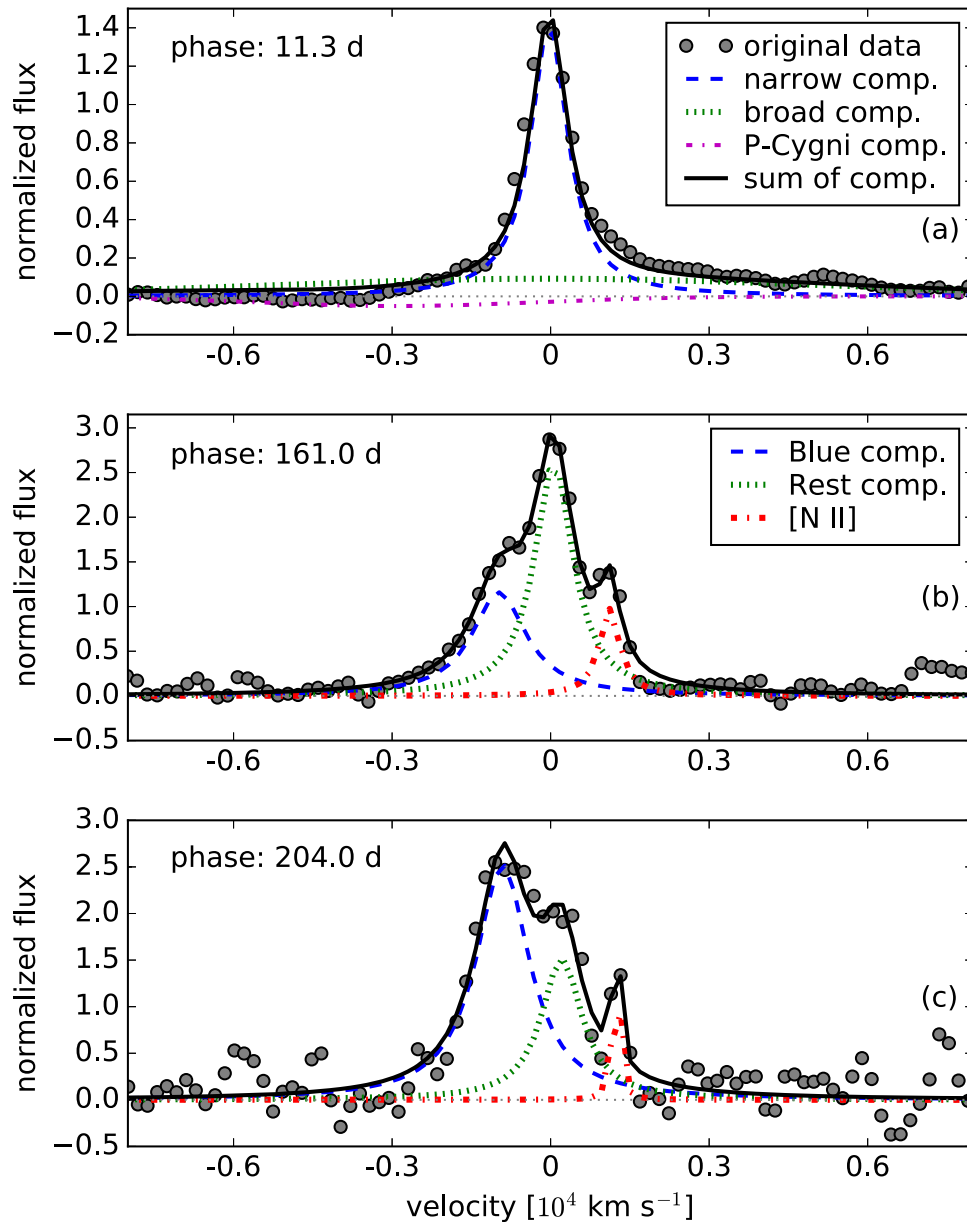


Figure 9. Decomposition of the $H\alpha$ emission line of SN 2010bt at phases 11.3, 161.0, and 204.0 days from the assumed V -maximum date.

average value, $A_V^{\text{tot}} = 1.24 \pm 0.42$ mag (i.e., $E(B - V) = 0.40 \pm 0.15$ mag), as the extinction toward SN 2010bt.

We measured the brightness of the progenitor candidate using Dolphot, finding $m_{F606W} = 22.23 \pm 0.02$ mag (also reported in Table 9). Dolphot reported that the progenitor candidate has an “object type” flag of “1,” which means that the source is likely stellar. Additionally, the object had a “sharpness” and a “crowding” parameter²³ ~ 0 , further indicating that the detected source is point-like and “clean” (Dolphin 2000).

²³ The “sharpness” parameter indicates the reliability that a detected source is indeed point-like. It is considered a “good star” when this parameter is between -0.3 and $+0.3$ and a “perfectly fit star” when the value is 0. The “crowding” parameter is defined in magnitude and describes the measured quality brightness of a star. Isolated stars have a crowding value of zero. This value increases as more stars surround the star under study, contaminating the measurement. Hence, a low value increases the certainty of the measured stars.

Dolphot also detected the candidate in F330W, although the object type is “2,” indicating that the source is a star too faint for a PSF determination; the other two parameters indicated that this object is an otherwise good and clean source. The magnitude measured (via aperture photometry) in this filter is $m_{F330W} = 24.29 \pm 0.23$ mag. Note that the *HST* images taken with F606W were obtained in 1994 and those using F330W in 2003.

We obtained $m_{F606W} = 22.50 \pm 0.05$ mag for the SN, running Dolphot on the *HST* images taken on 2010 (assuming that the F606W bandpass is approximately Johnson V , we include this measurement in Table 3). The SN was therefore found to be slightly fainter than the progenitor candidate.

Finally, we ran Dolphot on the 2015 late-time *HST* images of the SN field. By adding artificial stars at the SN position, we obtained conservatively an upper brightness limit for a single point source with a sigma threshold of 3.0 of $m_{F555W} \gtrsim 24.4$

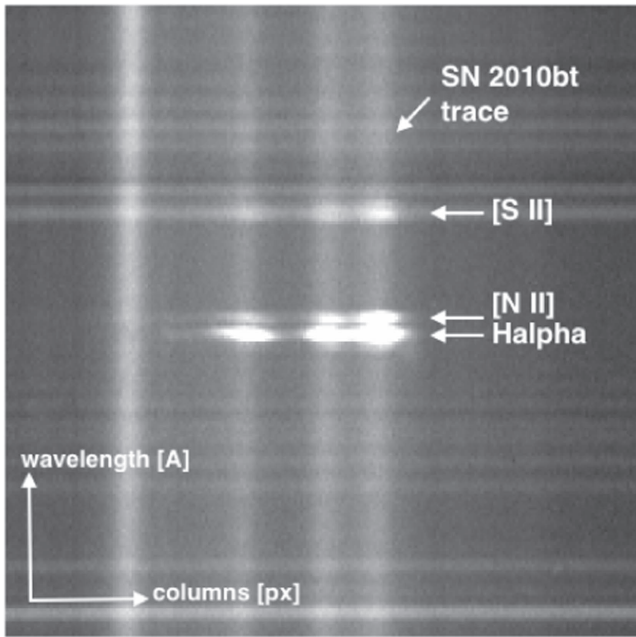


Figure 10. $H\alpha$ emission line in the 2D spectrum of SN 2010bt taken with NTT+EFOSC2 on 2010 September 15 (phase 161.0 days from the assumed V -maximum date).

Table 9
SN 2010bt and the Progenitor Candidate Position Comparison

	F330W (α/δ)	F606W (α/δ)	F555W (α/δ)
Total uncertainty (mas)	10/10	9/8	10/10
Diff. position SN/candidate (mas)	28/7	13/8	...

Note. Uncertainties are 1σ .

mag. That is, the previously identified source had disappeared, being at least 2 mag fainter than in the observations in 1994. The precise match between the *HST* images taken before and after the SN explosion, the fit quality given by Dolphot, and the disappearance of the progenitor star 5 yr after the explosion tell us that this star is likely the progenitor of SN 2010bt. Note that the 2015 *HST* images were obtained with WFC3, which has better throughput than WFPC2. SN 2009ip was also observed at late time phases (>1100 days after the maximum of its brightest event 2012b), at which time the luminosity of the transient was probably still dominated by CSM interaction, and was found to be marginally fainter than its quiescent progenitor (Thöne et al. 2015; Smith et al. 2016; Graham et al. 2017). Unfortunately, like SN 2009ip, then, this apparent fading of SN 2010bt 15 yr after the nominally SN-like event cannot alone prove that it was a terminal explosion.

Correcting by the total extinction and distance assumed for the SN (see the beginning of this section and Section 1), we find that the absolute magnitude of the progenitor was $M_{F606W}^0 = -12.98 \pm 0.41$ mag and $M_{F330W}^0 = -11.82 \pm 0.74$ mag, while the SN was at -12.72 ± 0.42 mag (F606W) in 2010 and $\gtrsim -11$ mag (F555W) in 2015.

Adopting zero bolometric correction and that $m_{F606W} \approx V$, we find that the progenitor candidate has a bolometric luminosity of $\log(L/L_\odot) \approx 7.1 \pm 0.2$. Such a luminosity is too large for a star in quiescence, and thus it is more likely that

Table 10
Brightness^a of SN 2010bt and the Progenitor Candidate

	F330W (mag)	F606W (mag)	F555W (mag)
Progenitor candidate	24.29 (0.23) ^b	22.23 (0.02) ^c	...
SN 2010bt	...	22.50 (0.05) ^d	$\gtrsim 24.4$ ^e

Notes.

^a Magnitude uncertainties are 1σ .

^b Image taken with *HST*+ACS/HRC on 2003 May 08.

^c Image taken with *HST*+WFPC2 on 1994 August 23.

^d Image taken with *HST*+ACS/WFC on 2010 October 09.

^e Image taken with *HST*+WFC3/UVIS on 2015 October 14.

the progenitor was observed in eruption at that epoch.²⁴ Curiously, this value of luminosity is evocative of η Carinae during its Great Eruption (Humphreys et al. 1999; Rest et al. 2012; see also Figure 12).

It is well known that the surrounding medium of a star can affect the peak luminosity and spectra during the explosion. Indeed, SN 2010bt was classified as Type IIn owing to the presence of narrow circumstellar H emission. A possible explanation for the fact that the SN light faded so drastically in just a few months after the explosion could be the result of possible formation of dust in the ejected material, which could have obscured the SN light (or the “remnant” if it survived the explosion). In this case, we should expect at late times a strong IR excess, as in the case of SN 1998S (Pozzo et al. 2004) or SN 2005ip (e.g., Smith et al. 2009; Fox et al. 2010). Therefore, we analyzed several sets of IR images obtained with the InfraRed Array Camera (IRAC) on board the *Spitzer Space Telescope*, before (2004 October 30; 3.6, 4.5, 5.8, and 8 μ m channels; PI: J.M. Mazzarella; Program ID 3672) and after (2012–2015; 3.6, and 4.5 μ m channels; PIs D.B. Sanders, O.D. Fox, D. Stern; Program IDs 80089, 90031, 10098, respectively) the SN explosion. We worked with the post-basic calibrated data (PBCD) provided by the *Spitzer* Heritage Archive,²⁵ which are already fully co-added and calibrated. Neither the progenitor candidate nor SN 2010bt was detected in any *Spitzer* channel (see Figure 13). We therefore attempted to constrain the dust formation at the SN site by measuring the variance of the integrated flux in an area of 3×3 pixels around the progenitor/SN position using MOPEX. Following the “recipe” advised by the *Spitzer* team, we obtained the upper limits reported in Table 11.

As one can see, there is no evidence of IR excess emission from years 2004 through 2014. The upper limits on the IR emission from SN 2010bt tell us that there are no detections larger than $\sim 9 \times 10^{40}$ erg s⁻¹ and $\sim 7 \times 10^{40}$ erg s⁻¹ at 3.6 and 4.5 μ m, respectively. Thus, it is quite likely that the drop in luminosity of SN 2010bt is not caused by dust formation, but rather by the end of the ejecta interaction with the CSM.

5. Was SN 2010bt a Nonterminal Explosion?

As discussed by many authors, the dividing line between SN impostors and real SNe is not clear, with both possibilities viable for several objects. Both families of transients share

²⁴ Assuming $A_V^{\text{tot}} = 0$ mag, the bolometric luminosity of SN 2010bt’s progenitor is $\log(L/L_\odot) \approx 6.8 \pm 0.1$. This luminosity is still more appropriate for a star in eruption.

²⁵ <http://sha.ipac.caltech.edu/applications/Spitzer/SHA/>

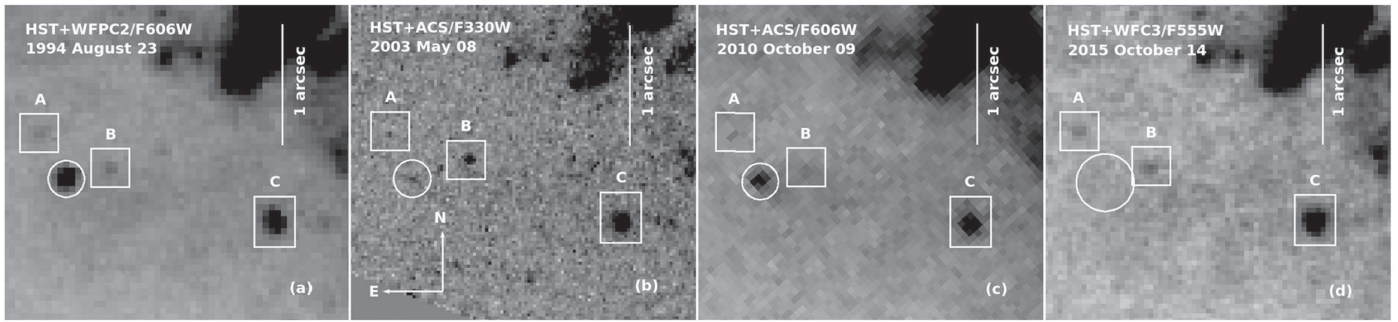


Figure 11. Subsections of the NGC 7130 pre-explosion (a) *HST* WFPC2 image in F606W and (b) *HST* ACS/HRC image in F330W, along with (c) the post-explosion *HST* ACS/WFC image of the SN site in F606W and (d) the late-time *HST* WFC3/UVIS image in F555W. The positions of the SN candidate progenitor and SN are indicated by circles, each with a radius of 3 pixels (between $0''.08$ and $0''.15$), except in panel (d), for which the radius is 6 pixels ($\sim 0''.23$). The positions of three neighboring sources of SN 2010bt (“A,” “B,” and “C”) are also indicated.

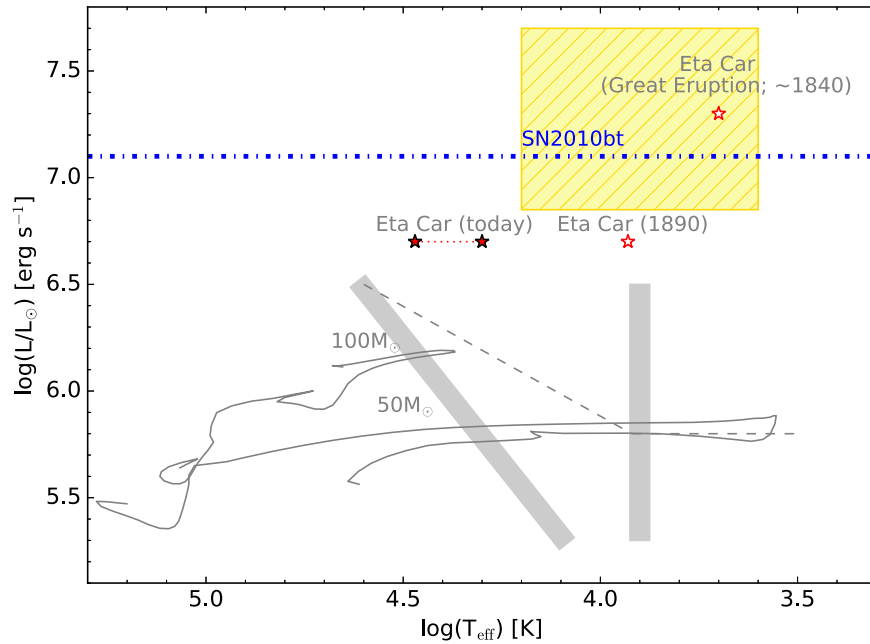


Figure 12. Hertzsprung–Russell diagram showing the luminosity (dot-dashed horizontal line) of the source found at the SN 2010bt position in pre-explosion *HST* images. For comparison, we also display the loci of the η Carinae eruptions. The yellow (light) shaded area highlights the approximate region during the progenitor outburst phase of SN 2009ip (Smith et al. 2010, 2014; Foley et al. 2011), UGC 2773-OT (Smith et al. 2010), SNhunt248 (Kankare et al. 2015), PSN J09132750 +7627410 (Tartaglia et al. 2016), and SN 2015bh (Elias-Rosa et al. 2016; Thöne et al. 2017). Note that the color of the SN 2009ip progenitor is poorly constrained, since it was observed with only one filter. The gray (darker) shaded bands indicate the typical locations of luminous blue variables in quiescence (left, diagonal band) and during the S-Doradus-like variability (vertical band). The dashed line indicates the Humphrey–Davidson instability limit (Humphreys & Davidson 1994). We also show evolutionary tracks at $50 M_{\odot}$ and $100 M_{\odot}$ from the Cambridge STARS (Eldridge & Tout 2004) models, assuming solar metallicity.

observable similarities; however, the big difference is in the progenitor star fate—the star is destroyed in an SN explosion, but it still remains after the outburst in the case of an SN impostor. It is also hard to find a unique origin of SN 2010bt. We discuss below the observables of this transient.

1. Both early and late spectra show spectra dominated by strong multicomponent Balmer emission lines, indicators that define the interacting transients. The $H\alpha$ profile of SN 2010bt at early time resembles more those of the interacting transients, such as SN 2009ip and SN 2015bh, than those of confirmed SNe IIn SN 1996al and SN 1998S (see Section 2.2). Instead, at late phases, none of the comparison transients share the same $H\alpha$ profile as SN 2010bt. This is understandable since the CSM may evolve in a different way for each object, leading to diversity among the transients.

2. Photometrically (see Section 2.1), SN 2010bt exhibits a rapid decrease in luminosity after maximum, which is reminiscent of the SN 2009ip-like objects, and is somehow faster than other SNe. However, the luminosity at maximum of SN 2010bt is higher than that of SN 2009ip and most consistent with the peak luminosity of bright SNe IIn.
3. The flattening of the late-time light curve seems slower than that expected for interacting SNe; however, it is still at the low end of the typical ^{56}Ni mass range for CC-SNe. It is, however, in agreement with what was estimated for SN 2009ip-like SNe.
4. Considering the pseudobolometric luminosity of SN 2010bt, we estimate a radiated energy of at least 2×10^{49} erg. This energy is comparable to that of SNe IIn (e.g., Arnett 1996), but also to major eruptive events of some transients, such as SN 2009ip ($\sim 3 \times 10^{49}$ erg; Margutti et al. 2014).

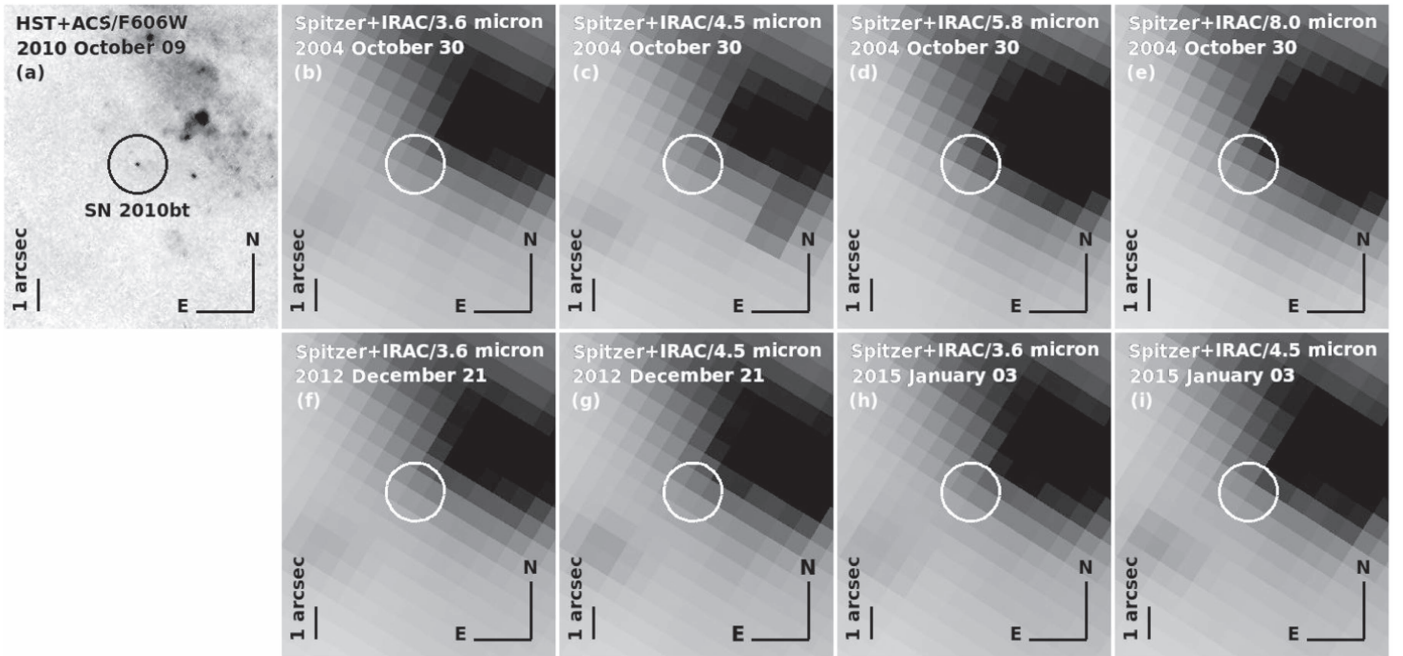


Figure 13. Subsections of (a) the post-explosion *HST* ACS/WFC image in F606W, along with (b)–(i) a sample of archival *Spitzer* images in different channels and epochs. The position of the SN is indicated by circles with a radius of 18 pixels ($0''.9$) for the *HST* image and 1.5 pixels ($0''.9$) for the *Spitzer* images.

Table 11
Spitzer Flux Upper Limits at the SN 2010bt Site

Date	MJD	Phase ^a (days)	3.6 μm (μJy)	4.5 μm (μJy)	5.8 μm (μJy)	8.0 μm (μJy)	Program ID
20041030	53,308.2	−1994.9	<195.5	<196.2	<749.2	<2560.0	3672
20121221	56,282.7	979.5	<202.6	<209.7	80089
20121221	56,282.9	979.8	<169.3	90031
20130123	56,315.5	1012.4	<205.3	90031
20130718	56,491.4	1188.3	<177.3	90031
20130820	56,524.2	1221.1	<238.7	90031
20131224	56,650.4	1347.3	<223.1	90031
20140131	56,688.6	1385.5	<210.1	90031
20140727	56,865.9	1562.8	<193.8	90031
20140829	56,898.4	1595.3	<197.5	90031
20150103	57,025.9	1722.8	<237.6	<177.5	10098

Note.

^a Phases are relative to the discovery date, MJD = 55,303.1.

- Unfortunately, except for the estimated magnitude of the progenitor star, we have not found any other data indicative of a possible pre-SN eruptive event.
- We estimated an absolute magnitude for the progenitor star of $M_{F606W}^0 \simeq -12.3$ mag (see Section 4), which is similar to that derived for the SN in 2010, -12.7 mag (F606W). That luminosity is more like that of a star in outburst, if we compare with SN impostors, such as UGC 2773-OT (Smith et al. 2010), SNhunt248 (Kankare et al. 2015), or PSN J09132750+7627410 (Tartaglia et al. 2016), which were all between -13 and -14 mag, or objects in outburst, such as SN 2009ip (e.g., Pastorello et al. 2013), SN 2015bh (Elias-Rosa et al. 2016; Thöne et al. 2017), or η Carinae during its Great Eruption (Humphreys et al. 1999; Rest et al. 2012). Note also that the progenitor luminosity found for the SN II in 2005gl

- (Gal-Yam et al. 2007; Gal-Yam & Leonard 2009), or some SN 2009ip-like transients (Smith et al. 2010, 2014; Foley et al. 2011; Elias-Rosa et al. 2016; Pastorello et al. 2018), is around ~ -10 mag.
- Several years after the discovery, the progenitor of SN 2010bt seems to have vanished, indicating that the star may have finally exploded as an SN (see Section 4). This has been inferred for interacting SNe, such as SN 2005gl, but not yet for any member of the SN 2009ip-like family. As discussed by Pastorello et al. (2018), SN 2009ip-like transients share similarities with SN 2005gl, supporting the possible terminal explosion scenario for all.

In short, the SN 2010bt observations have not helped us clarify whether the transient is an SN or an impostor, with the

exception of the very late-time *HST* data that may show that the progenitor had vanished. It makes the terminal explosion scenario plausible for this event.

6. Summary

SN 2010bt was classified as an SN II_n from an optical spectrum taken not long after the explosion. The observational campaign was interrupted after ~ 2 months, owing to the SN's proximity to the Sun in the sky, and was again continued just a few months later. By that time, the SN had become much fainter or was nearly undetectable, which is unusual behavior for an SN in general. SN detection at late phases was obtained only through images taken with *HST*, at a luminosity of ~ -12.7 mag in the F606W band.

Comparing *HST* images of the host galaxy prior to the explosion and those of the SN at late times, high-precision relative astrometry allowed us to identify the likely SN progenitor star with magnitude ~ -13 in the F606W band, which is almost certainly the luminosity of a star in eruption. At first we found that the brightness of the SN nearly 5 months after discovery was somewhat smaller than that estimated for the progenitor candidate. Still, no source more luminous than -11 mag in the F555W band was found at the position of the SN 5 yr after the SN discovery.

Overall, we have not found a unique explanation for the chain of events observed for SN 2010bt. In the following we will list our best understanding of the transient's observables.

1. The SN 2010bt progenitor, identified in the *HST* pre-SN images, was in outburst ($M_{F606W}^0(\sim V) \approx -13$ mag; $\log(L/L_{\odot}) \approx 7$) at the moment of the observations in 1994. Unfortunately, no information about other possible pre-SN eruptive events has been found.
2. Some time thereafter, a powerful (terminal or nonterminal) outburst occurs, resulting in SN 2010bt.
3. The ejecta interacted with a compact shell created during eruptions or heavy mass loss from the massive progenitor star prior to the explosion. This shock/CSM interaction led to SN 2010bt reaching a quite luminous $M_V \geq -19$ mag.
4. A probably patchy photosphere is located in the external symmetric CSM, where the CSM–ejecta interaction is taking place, since the early-time observed $H\alpha$ profile is quite symmetric and a weak broad component is visible.
5. The CSM+ejecta recombined quickly, leading to the observed rapid decline of the SN 2010bt light curve.
6. The ejecta continued to propagate into more distant CSM. This probably had an asymmetric geometry, since the late-time $H\alpha$ emission showed a double-peaked profile.
7. Over time, the CSM–ejecta interaction became far less strong; consequently, we saw no further trace of SN 2010bt (at least not brighter than -11 mag) in 2015.

In conclusion, we confirm the identification of the SN 2010bt progenitor in outburst and favor the scenario in which SN 2010bt was a genuine SN surrounded by dense CSM with a complex geometry.

N.E.-R. thanks Avet Harutyunyan for his help and acknowledges the hospitality of the Institut de Ciències de l'Espai at the Autonomous University of Barcelona's Campus, where much of this work was written. Support for this work

was provided by NASA/*HST* through grants GO-11575, GO-13684, GO-14668, and AR-14295 from the Space Telescope Science Institute (STScI), which is operated by AURA, Inc., under National Aeronautics and Space Administration (NASA) contract NAS5-26555. S.B. and M.T. acknowledge partial financial support by the PRIN-INAF 2017 (project “Towards the SKA and CTA Era: Discovery, Localization, and Physics of Transient Sources”). A.V.F. is grateful for generous financial assistance from the Christopher R. Redlich Fund, the TABASGO Foundation, the Miller Institute for Basic Research in Science (UC Berkeley), and US NSF grant AST-1211916. G.P. acknowledges support provided by the Millennium Institute of Astrophysics (MAS) through grant IC120009 of the Programa Iniciativa Científica Milenio del Ministerio de Economía, Fomento y Turismo de Chile. L.G. was supported in part by NSF grant AST-1311862. N.S. was supported in part by NSF grants AST-1312221 and AST-1515559. This research is based in part on observations made with the NASA/ESA *Hubble Space Telescope* and obtained from the Hubble Legacy Archive, which is a collaboration between STScI/NASA, the Space Telescope European Coordinating Facility (ST-ECF/ESA), and the Canadian Astronomy Data Centre (CADC/NRC/CSA); the *Spitzer Space Telescope*, which is operated by the Jet Propulsion Laboratory, California Institute of Technology, under a contract with NASA (support was provided by NASA through an award issued by JPL/Caltech); the SMARTS Consortium 1.3 m telescope located at Cerro Tololo Inter-American Observatory (CTIO), Chile; and the New Technology Telescope at the European Southern Observatory–La Silla Observatory. Data in this work have been taken in the framework of the European supernova collaboration involved in ESO-NTT large program 184.D-1140 led by Stefano Benetti. Many of the spectra used here for comparison were obtained from the Padova-Asiago Supernova Archive (ASA). This work has made use of the NASA/IPAC Extragalactic Database (NED), which is operated by the Jet Propulsion Laboratory, California Institute of Technology, under contract with NASA, and data products from the Two Micron All Sky Survey, which is a joint project of the University of Massachusetts and the Infrared Processing and Analysis Center/California Institute of Technology, funded by NASA and the NSF.

Facilities: *Swift*, *Spitzer*, ING:Kapteyn (JAG), CTIO:1.3m (ANDICAM), *HST*(WFPC2), ACS, WFC3, ESO:3.6m (EFOSC2, SOFI), Magellan:Clay (LDSS-3), VLT:Yepun (HAWK-I).

Software: IRAF (Tody 1986, 1993), SNOOPY (<http://sngroup.oapd.inaf.it/snoopy.html>), SExtractor (Bertin & Arnouts 1996), HOTPANTS (Becker 2015), Dolphot (Dolphin 2000), GELATO (<https://gelato.tng.iac.es>), MOPEX (<http://irsa.ipac.caltech.edu/data/SPITZER/docs/dataanalysis/tools/mopex/>).

ORCID iDs

Nancy Elias-Rosa  <https://orcid.org/0000-0002-1381-9125>
Schuyler D. Van Dyk  <https://orcid.org/0000-0001-9038-9950>

Enrico Cappellaro  <https://orcid.org/0000-0001-5008-8619>
Rubina Kotak  <https://orcid.org/0000-0001-5455-3653>

Alexei V. Filippenko  <https://orcid.org/0000-0003-3460-0103>

Giuliano Pignata  <https://orcid.org/0000-0003-0006-0188>
Ori D. Fox  <https://orcid.org/0000-0003-2238-1572>

Lluís Galbany  <https://orcid.org/0000-0002-1296-6887>
 Santiago González-Gaitán  <https://orcid.org/0000-0001-9541-0317>

References

- Anderson, J. P., González-Gaitán, S., Hamuy, M., et al. 2014, *ApJ*, **786**, 67
- Arnett, D. 1996, *Supernovae and Nucleosynthesis* (Princeton, NJ: Princeton Univ. Press)
- Becker, A. 2015, HOTPANTS: High Order Transform of PSF ANd Template Subtraction, Astrophysics Source Code Library, ascl:1504.004
- Benetti, S., Chugai, N. N., Utrobin, V. P., et al. 2016, *MNRAS*, **456**, 3296
- Bertin, E., & Arnouts, S. 1996, *A&AS*, **117**, 393
- Blanton, M. R., & Roweis, S. 2007, *AJ*, **133**, 734
- Brown, P. J., Breeveld, A. A., Holland, S., Kuin, P., & Pritchard, T. 2014, *Ap&SS*, **354**, 89
- Cardelli, J. A., Clayton, G. C., & Mathis, J. S. 1989, *ApJ*, **345**, 245
- Chugai, N. N., & Danziger, I. J. 1994, *MNRAS*, **268**, 173
- de Vaucouleurs, G., de Vaucouleurs, A., & Corwin, J. R. 1976, *Second Reference Catalogue of Bright Galaxies* (Austin, TX: Univ. Texas Press)
- Dolphin, A. E. 2000, *PASP*, **112**, 1383
- Dwek, E., Arendt, R. G., Fox, O. D., et al. 2017, *ApJ*, **847**, 91
- Eldridge, J. J., & Tout, C. A. 2004, *MNRAS*, **353**, 87
- Elias-Rosa, N., Pastorello, A., Benetti, S., et al. 2016, *MNRAS*, **463**, 3894
- Fassia, A., Meikle, W. P. S., Vacca, W. D., et al. 2000, *MNRAS*, **318**, 1093
- Filippenko, A. V. 1982, *PASP*, **94**, 715
- Filippenko, A. V. 1997, *ARA&A*, **35**, 309
- Foley, R. J., Berger, E., Fox, O., et al. 2011, *ApJ*, **732**, 32
- Fox, O. D., Chevalier, R. A., Dwek, E., et al. 2010, *ApJ*, **725**, 1768
- Fox, O. D., Van Dyk, S. D., Dwek, E., et al. 2017, *ApJ*, **836**, 222
- Fraser, M., Inserra, C., Jerkstrand, A., et al. 2013, *MNRAS*, **433**, 1312
- Galbany, L., Hamuy, M., Phillips, M. M., et al. 2016, *AJ*, **151**, 33
- Gal-Yam, A., & Leonard, D. C. 2009, *Natur*, **458**, 865
- Gal-Yam, A., Leonard, D. C., Fox, D. B., et al. 2007, *ApJ*, **656**, 372
- Graham, M. L., Bigley, A., Mauerhan, J. C., et al. 2017, *MNRAS*, **469**, 1559
- Hamuy, M. 2003, *ApJ*, **582**, 905
- Hamuy, M., Suntzeff, N. B., Heathcote, S. R., et al. 1994, *PASP*, **106**, 566
- Hamuy, M., Walker, A. R., Suntzeff, N. B., et al. 1992, *PASP*, **104**, 533
- Home, K. 1986, *PASP*, **98**, 609
- Humphreys, R. M., & Davidson, K. 1994, *PASP*, **106**, 1025
- Humphreys, R. M., Davidson, K., & Smith, N. 1999, *PASP*, **111**, 1124
- Kankare, E., Kotak, R., Pastorello, A., et al. 2015, *A&A*, **581**, L4
- Kiewe, M., Gal-Yam, A., Arcavi, I., et al. 2012, *ApJ*, **744**, 10
- Leonard, D. C., Filippenko, A. V., Barth, A. J., & Matheson, T. 2000, *ApJ*, **536**, 239
- Li, W., Leaman, J., Chornock, R., et al. 2011, *MNRAS*, **412**, 1441
- Liu, Q.-Z., Hu, J.-Y., Hang, H.-R., et al. 2000, *A&AS*, **144**, 219
- Margutti, R., Milisavljevic, D., Soderberg, A. M., et al. 2014, *ApJ*, **780**, 21
- Mauerhan, J., & Smith, N. 2012, *MNRAS*, **424**, 2659
- Mauerhan, J. C., Smith, N., Filippenko, A. V., et al. 2013, *MNRAS*, **430**, 1801
- Miluzio, M., Cappellaro, E., Botticella, M. T., et al. 2013, *A&A*, **554**, A127
- Monard, L. A. G. 2010, *CBET*, **2250**, 1
- Mould, J. R., Huchra, J. P., Freedman, W. L., et al. 2000, *ApJ*, **529**, 786
- Ofek, E. O., Arcavi, I., Tal, D., et al. 2014, *ApJ*, **788**, 154
- Oke, J. B. 1990, *AJ*, **99**, 1621
- Pastorello, A., Botticella, M. T., Trundle, C., et al. 2010, *MNRAS*, **408**, 181
- Pastorello, A., Cappellaro, E., Inserra, C., et al. 2013, *ApJ*, **767**, 1
- Pastorello, A., Kochanek, C. S., Fraser, M., et al. 2018, *MNRAS*, **474**, 197
- Phillips, M. M., Charles, P. A., & Baldwin, J. A. 1983, *ApJ*, **266**, 485
- Phillips, M. M., Simon, J. D., Morrell, N., et al. 2013, *ApJ*, **779**, 38
- Poznanski, D., Prochaska, J. X., & Bloom, J. S. 2012, *MNRAS*, **426**, 1465
- Pozzo, M., Meikle, W. P. S., Fassia, A., et al. 2004, *MNRAS*, **352**, 457
- Rest, A., Prieto, J. L., Walborn, N. R., et al. 2012, *Natur*, **482**, 375
- Schlegel, E. M. 1990, *MNRAS*, **244**, 269
- Smith, N. 2014, *ARA&A*, **52**, 487
- Smith, N., Andrews, J. E., & Mauerhan, J. C. 2016, *MNRAS*, **463**, 2904
- Smith, N., Li, W., Filippenko, A. V., & Chornock, R. 2011a, *MNRAS*, **412**, 1522
- Smith, N., Li, W., Miller, A. A., et al. 2011b, *ApJ*, **732**, 63
- Smith, N., Li, W., Silverman, J. M., Ganeshalingam, M., & Filippenko, A. V. 2011c, *MNRAS*, **415**, 773
- Smith, N., Mauerhan, J. C., & Prieto, J. L. 2014, *MNRAS*, **438**, 1191
- Smith, N., Miller, A., Li, W., et al. 2010, *AJ*, **139**, 1451
- Smith, N., Silverman, J. M., Chornock, R., et al. 2009, *ApJ*, **695**, 1334
- Smith, N. 2017, in *Handbook of Supernovae*, ed. A. W. Alsabti & P. Murdin (Berlin: Springer), 403
- Taddia, F., Stritzinger, M. D., Sollerman, J., et al. 2013, *A&A*, **555**, A10
- Tartaglia, L., Elias-Rosa, N., Pastorello, A., et al. 2016, *ApJL*, **823**, L23
- Tartaglia, L., Pastorello, A., Taubenberger, S., et al. 2015, *MNRAS*, **447**, 117
- Thöne, C., de Ugarte Postigo, A., Leloudas, G., Cano, Z., & Maeda, K. 2015, *ATel*, **8417**, 1
- Thöne, C. C., de Ugarte Postigo, A., Leloudas, G., et al. 2017, *A&A*, **599**, A129
- Tody, D. 1986, *Proc. SPIE*, **627**, 733
- Tody, D. 1993, in *ASP Conf. Ser. 52, Astronomical Data Analysis Software and Systems II*, ed. R. J. Hanisch, R. J. V. Brissenden, & J. Barnes (San Francisco, CA: ASP), 173
- Turatto, M., Benetti, S., & Cappellaro, E. 2003, in *From Twilight to Highlight: The Physics of Supernovae*, ed. W. Hillebrandt & B. Leibundgut (Berlin, Springer), 200
- Turatto, M., Benetti, S., Cappellaro, E., & Bufano, F. 2010, *CBET*, **2252**, 1
- Turatto, M., Cappellaro, E., Danziger, I. J., et al. 1993, *MNRAS*, **262**, 128
- Van Dyk, S. D., & Matheson, T. 2012, in *Eta Carinae and the Supernova Impostors*, ed. K. Davidson & R. M. Humphreys (New York: Springer), 249
- Van Dyk, S. D., Peng, C. Y., King, J. Y., et al. 2000, *PASP*, **112**, 1532
- Yaron, O., & Gal-Yam, A. 2012, *PASP*, **124**, 668